Cold forming of Al-5251 and Al-6082 tailored welded blanks manufactured by laser and electron beam welding

Himanshu Lalvani[1], Paranjayee Mandal[2,*]

himanshu.lalvani@strath.ac.uk[1], paranjayee.mandal@strath.ac.uk[2]

Advanced Forming Research Centre (AFRC) at National Manufacturing Institute Scotland (NMIS), University of Strathclyde, 85 Inchinnan Drive, Renfrew, PA4 9LJ, UK

*Corresponding author, ORCID id: 0000-0002-8440-703X

Abstract

This work demonstrates applicability of electron beam welding (EBW) and laser beam welding (LBW) techniques for manufacture of tailored welded blanks (TWBs) from Al-5251 (H22) and Al-6082 (T6) sheets. A combination of dissimilar sheets as well as thicknesses (1.5 mm and 2.5 mm) has been used in addition to a similar combination. An optimal post-weld heat treatment (PWHT) was determined that was effective in relieving stresses and impart adequate ductility in the TWBs allowing cold forming (i.e. stamping), into a cruciform geometry, at ambient temperature. Pull tests revealed marked improvement in elongation for all the welds, including all combinations, after PWHT. Micro-hardness mapping of the weld sections showed transition from a non-uniform to a more uniform distribution via slight increase in hardness of the weld region whilst decrease in the hardness of the parent materials. Non-contact optical measurement using GOM camera showed minimal localised thinning in steep angled areas of the cruciform geometry. The dissimilar LBW TWBs, after PWHT, showed noticeable increase in elongation, homogeneous hardness distribution and slightly refined microstructure in the fusion zone (FZ) compared to their EBW counterparts.

Keywords:

Tailor welded blanks (TWBs); Aluminium alloys; Electron beam welding (EBW); Laser beam welding (LBW); post-weld heat treatment (PWHT); Cold forming; Stamping; Weld microstructure;

Graphical abstract

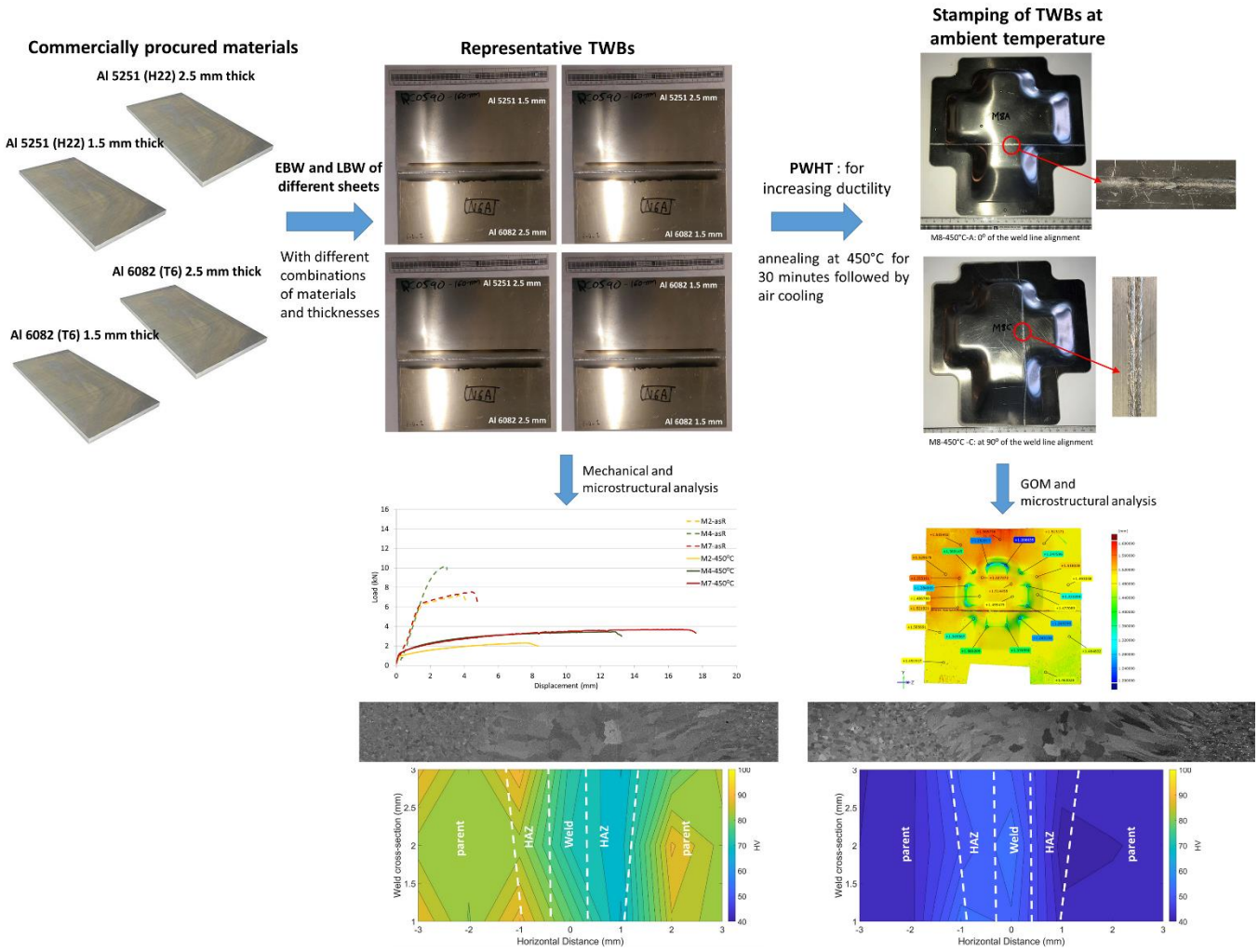

1. Introduction

Reduced vehicle weight and lower manufacturing costs are two apparently conflicting requirements, which connect the restricted fuel economy with the growing economic competition in both automotive and aerospace sectors. The conventional assembly methods consisting of several stamping operations followed by spot welding and/or riveting, often fail to meet those requirements, however the tailor welded blanks (TWBs) successfully address those issues. Hovanski et al. [1] and Parente et al. [2] summarised the advantages of TWBs over conventional assembly methods in terms of – (i) weight reduction by welding different sheet thicknesses, (ii) cost reduction by using less forming dies, (iii) maintaining dimensional consistency, corrosion resistance and strength requirements by eliminating lap joints and substituting conventional spot welds with laser and mash seam welds, (iv) overall material

optimisation by varying material composition, local or global heat-treatment and application of surface coatings. A TWB is basically a preform made of two or more separate sheet metal pieces welded together with an objective of achieving benefits of combined properties of different sheets, which are either different alloys or have different thicknesses. The TWB is then hot or cold formed into the final net shaped component using a single metal forming press. TWBs are typically made from steel using laser welding process and have widespread application in both automotive and construction sectors due to their good formability and strength as described by Pallett and Lark [3]. Lutsey [4] reported that a fuel saving of ~5 – 7% and a vehicle weight reduction of ~10% is possible by using lightweight materials, particularly Al, as compared to the steel body structure. As a result, sufficient attention has been paid to manufacturing the TWBs from dissimilar materials such as, Steel-Al pair, as well as dissimilar Al alloys particularly for automotive applications. Mao and Altan [5] summarised the most commonly used 5000 and 6000 series Al alloys in automotive parts, such as hoods, trunk lids, inner and outer panel doors and side frames of a car body to name a few. The work hardened 5000 series Al alloys (Al-Mg alloys) are non-heat treatable but have relatively good formability and ultimate tensile strength (UTS) in the range of 125 – 350 MPa. They are typically used for inner panel door applications (particularly Al-5182 and Al-5754) due to Lüders band formation during forming. On the other hand, the age hardened 6000 series Al alloys (Al-Mg-Si alloys) have UTS in the range of 125 – 400 MPa, good corrosion resistance and high strength to weight ratio under heat-treated conditions. The precipitation-hardening is caused by the Mg_2Si precipitates during heat treatment, which leads to increased strength level required for outer panel door applications (particularly Al-6022 and Al-6111).

Hovanski et al. [1] and Parente et al. [2] reviewed a number of fusion welding methods, such as tungsten inert gas (TIG) welding, gas tungsten arc welding (GTAW), laser beam welding (LBW), resistance mash welding, resistance spot welding (RSW), electron beam lding (EBW) and friction stir welding (FSW), employed to produce Al TWBs with a thickness range of 1 – 3 mm. All these techniques, except the FSW, involve localised melting and formation of heat affected zone (HAZ), which eventually lead to weld distortion, solidification cracking, porosity and thereby significant mismatch in the mechanical and microstructural properties between the weld and the parent materials. Initially, Huntington and Eagar [6] as well as Pastor et al. [7] mentioned restricted use of LBW during welding of Al alloys due to high surface reflectivity, high thermal conductivity, vaporisation of low melting point of constituents such as Mg and Zn, formation of brittle oxide layers, blow holes and porosity within the weld seam, and hot cracking of HAZ. Later these problems were mostly excluded by introduction of high power and high density CO_2 and Nd:YAG lasers with improved beam quality and beam focussing systems, which altogether enabled the welding of both 5000 and 6000 series Al alloys as pointed out by Verhaeghe [8]. Typically, LBW of Al alloys is performed in the keyhole mode due to its high welding speed (3 – 10 m/min) and the same was adopted by Venkat et al. [9] and Braun [10]. Venkat et al. [9] investigated the tensile, hardness and microstructural properties of the LBW butt joints individually

made of 1.63 mm thick Al-5754 (O) and 1.02 mm thick Al-6111 (T4) sheets. They reported solid welds for both alloys with reasonably higher elongation (>20%) observed for Al-5754. Both alloys showed mostly cellular dendritic microstructure in the fusion zone (FZ), however failure modes observed were different – ductile rupture for Al-5754, but both ductile rupture and brittle inter-dendritic failure for Al-6111. They also observed vaporization of strengthening elements from the HAZ, which then led to solidification cracking due to liquidation followed by re-solidification and significant reductions in the HAZ elongation. Likewise, Braun [10] inspected the tensile, hardness, microstructural and corrosion properties of LBW butt joint made of 1.6 mm thick Al-6013 (both T4 and T6) sheets with presence of different filler materials. Porosity was found to be the main weld defect in the FZ. Both FZ and partially melted zone (PMZ) exhibited cellular dendritic microstructure and an additional post-weld heat treatment (PWHT) to T6 condition (artificially aged at 191ºC for 4 hours) led to precipitation of strengthening phases. This resulted in significant improvements in hardness, ductility and corrosion resistance behaviour. The presence of porosity and therefore low hardness in FZ was also reported by Fabrègue et al. [11] during LBW of 2.5 mm thick Al-6056 (T4) butt joints using Al-4047 filler wire and by Pakdil et al. [12] during LBW of 6 mm thick Al-6056 (T6) T joints using AlSi12 filler wire. Although the keyhole mode cannot reduce the problem related to high surface reflectivity of Al alloys, but it can be eliminated either using a graphite based lubricant coating or using EBW simply being unresponsive to the surface reflectivity problems. Cam et al. [13] and Zhan et al. [14] summarised the advantages and disadvantages of EBW for welding of Al alloys over LBW, which involved better weld penetration, formation of narrow and contamination-free HAZ, reduced crack sensitivity, effective removal of brittle oxides, evaporation of strengthening elements like Mg leading to poor mechanical strength at the weld seam and high initial capital investment due to vacuum enclosure. Zhan et al. [15] compared the EBW and LBW techniques during welding of 3 mm thick Al-5A06 alloy sheets and concluded the benefits of EBW over LBW for short period of time. The cross-sectional area of weld seam was observed ~60% larger in LBW with presence of pores, large grains, and low hardness. But EBW resulted in a narrow dagger-shaped better quality weld seam with no porosity, small grains, high hardness, and tensile strength. Deschamps et al. [16] carried out the EBW of 7 mm thick hollow spheres of Al–4.5%Zn–1%Mg (T652) alloy, where the weld zone was consisted of randomly distributed heterogeneous grains (1–50 μm). A PWHT to T6 condition (full solution treatment at 465ºC for 35 min, followed by air cooling) led to homogeneous microstructure with smaller precipitates and no detectable micro-segregation, but a lower hardness due to Zn evaporation. Overall, the application of EBW is restricted due to longer cycle times, size restrictions due to vacuum chamber, requirements for occupational safety (due to X ray generation) and cost of complex tooling instead of producing better quality welds than LBW. In this context, Mishra and Ma [17] and Threadgill et al. [18] described FSW as the most advantageous, energy efficient and matured solid-state joining process for particularly all types of Al alloys, which was benefitted by low heat input, high welding speed, flexibility of work piece geometry and ability to produce straight long distance butt joints or overlapped joints.

Both 5000 and 6000 series Al alloys are mostly weldable, however TWI [19] pointed out general problems related to welding of individual 5000 and 6000 series Al alloys – (i) softening of the HAZ in 5000 series Al alloys and (ii) local reduction of strength in 6000 series Al alloys due to redistribution of hardening precipitates within the HAZ. Threadgill et al. [18] mentioned that the heat input during welding allowed thermal recovery and recrystallization of the intensely deformed weld region in non-heat treatable 5000 series, whereas dissolution, re-precipitation and over-aging occurred for heat treatable 6000 series. As a result, attention has been paid particularly on dissimilar joining of these two alloy series due to their remarkably different forming and welding behaviour. For example, Mossman and Lippold [20] assessed the weldability of similar and dissimilar combinations of Al-6111 (T4), Al-6022 (T4), Al-5182 (H16), and Al-5754 (O) alloy sheets with 1 mm thickness using GTAW and determined the relative cracking susceptibility of the individual alloys as well as their combinations. They reported highest cracking resistance for dissimilar combinations of Al-5182 – Al-6111 and Al-5754 – Al-5182, whereas all combinations with Al-6022 showed an increased susceptibility to weld cracking. They observed non-uniform mixing at the fusion zone of the dissimilar combinations due to high travel speeds and differences in viscosity and surface tension, which led to a significant difference in the grain size from FZ to PMZ in HAZ. This difference in grain size also triggered failures fully contained within FZ and PMZ. Soundararajan et al. [21] showed FSW of Al-5182 and Al-6022 sheets with 2 mm thickness and evaluated the mechanical and microstructural properties of the lap weld as a function of the welding parameters. The process optimisation was achieved after extensive experimentation for 6022-top and 5182-bottom lap joint combination. The high temperature was particularly noted at the advancing side, where the weld failure occurred at the retreating side. A significant improvement in the weld strength was observed particularly for the dissimilar alloy combination as compared to the similar alloy combination. Costa et al. [22] also concluded that superior weld properties were obtained independent of the tool geometry when the lap joint was prepared using FSW of Al-6082 (T6)-top and Al-5754 (H22)-bottom combination for 1 mm sheet thickness. They studied the influence of hooking defect on the weld strength related to parent material positioning and properties. The hooking formation was strongly influenced by the tool shoulder plunge depth and the base material positioning, but the shape and size of hooking defect could be limited by controlling the upward flow of the lower plate material. Leitão et al. [23] studied the formability of 1 mm thick Al-5182 (H111) and Al-6016 (T4) sheets obtained by FSW. They observed that the initial blank size and the mismatch in mechanical properties between the weld and the parent materials strongly influenced the TWB formability. The formability was further verified by stamping of 180 mm and 200 mm diameter round TWBs into cylindrical cups, where the rupture was only observed under the presence of weld defects and non-uniform weld cross-section. Parente et al. [2] investigated the formability of 1 mm thick Al-5182 and Al-6061 (T651) sheets produced by FSW. The forming limit curves with Nakajima test results exhibited an increase in TWB formability with weld line aligned to rolling

direction, a decrease in TWB formability for the dissimilar pair as compared to the parent materials, significant loss of hardness in HAZ and presence of fracture sites in the weld zone towards Al-6061 side. Overall, these works indicate the widespread application of FSW in joining dissimilar 5000 and 6000 series Al alloys of same sheet thickness.

Unlike the TWBs produced using FSW, studies related to manufacturing of the dissimilar 5000 and 6000 series Al alloy TWBs using either LBW or EBW are scarce. Moreover, both EBW and LBW processes led to the poor mechanical properties at the weld zone (FZ and HAZ) without any PWHT when compared to FSW. For example, Siqueira et al. [24] compared the mechanical properties of different Al-7050, Al-2024, Al-2117 and Al-6013 T-joints prepared using riveting (maintaining military standard MS14218AD4-4), FSW and LBW. They concluded that both LBW and FSW could replace the riveting technique leading to higher tensile strength and toughness. They also observed the failure occurred far from the weld region for FSW but near to the bead for LBW. Lakshminarayanan and Balasubramanian [25] compared the FSW and EBW processes during butt joint of 4 mm thick cold rolled and annealed AISI 409M ferritic stainless steel. A higher tensile strength but slightly lower impact toughness was observed for FSW as compared to EBW. Therefore, a PWHT is required to improve the elongation prior to failure at the weld zone for both EBW and LBW processes.

The current work aims to understand manufacturability of thicker TWBs using EBW and LBW from dissimilar Al-5251 (H22) and Al-6082 (T6). Furthermore, cold formability of these TWBs has also been investigated through stamping trials. For this purpose, Al-5251 (H22) and Al-6082 (T6) alloy sheets were procured with two different thicknesses of 1.5 mm and 2.5 mm. Similar and dissimilar weld trials were carried out using the EBW and the LBW techniques to optimise weld process parameters. The TWBs were then manufactured using optimised weld parameters for both EBW and LBW. The TWBs, in as welded condition, were then put through stamping operation at ambient temperature resulting in cracking at the weld and in the parent sheet at locations of sharp transition. The initial results indicated requirement for an appropriate PWHT for imparting adequate ductility for subsequent stamping operation. The heat-treated TWBs were successfully stamped at AFRC's 500T hydraulic press, followed by detailed mechanical, microstructural and metrology analyses. The *novelty* of this work lies in establishing – (i) successful joining of dissimilar Al-5251 (H22) and Al-6082 (T6) sheets with different (i.e. 1.5 mm and 2.5 mm) thicknesses via both EBW and LBW, (ii) an appropriate PWHT to increase the formability of both similar and dissimilar TWBs for stamping operation at ambient temperature, (iii) successful stamping of TWBs into a cruciform geometry with low levels of localised thinning, minimal geometrical distortion and no cracking at weld or in parent sheets.

2. Materials and Manufacturing routes

2.1 Materials

The chemical compositions of both as-received materials, i.e. Al-5251 (H22, work hardened by rolling and partially annealed) and Al-6082 (T6, solution heat treated and artificially aged) sheets, are listed in Table 1. Each of the as-received sheet was received in two different thicknesses of 1.5 mm and 2.5 mm. The corresponding mechanical properties are provided in Table 2. These sheets were cut into appropriate rectangular sections, of 50 mm width and 120 mm length, using wire EDM (Electrical Discharge Machining) for sub-scale weld trials, using EBW and LBW processes, for parameter optimisation, mechanical testing and microstructure analysis. The full scale TWBs for, stamping trials, were manufactured from 150 mm width by 300 mm length sections making the final TWB dimension of 300 square mm.

Table 1: Chemical composition of the as-received Al-5251 (H22) and Al-6082 (T6) sheets

Al-5251 (H22) – 1.5 mm	Element	Si	Fe	Cu	Mn	Mg	Cr	Zn	Ti
	Wt%	0.1	0.38	0.01	0.29	2.05	0.01	0.01	0.01
	Element	Ni	Ga	V	Al				
	Wt%	0.05	0.01	0.02	balance				
Al-5251 (H22) – 2.5 mm	Element	Si	Fe	Cu	Mn	Mg	Cr	Zn	Ti
	Wt%	0.29	0.44	0.08	0.28	1.98	0.04	0.09	0.02
	Element	Ni	Ga	V	Al				
	Wt%	0.04	0.05	0.05	balance				
Al-6082 (T6) – 1.5 and 2.5 mm	Element	Si	Fe	Cu	Mn	Mg	Cr	Zn	Ti
	Wt%	0.9	0.35	0.07	0.45	0.7	0.02	0.03	0.04
	Element	Others	Al						
	Wt%	0.03	balance						

Table 2: Mechanical properties of the as-received Al-5251 (H22) and Al-6082 (T6) sheets

Materials	**Thickness of sheets (mm)**	**Yield strength (MPa) (0.2% proof stress)**	**Ultimate tensile strength (MPa)**	**% Elongation**
Al-6082 (T6)	1.5 and 2.5	300 ± 5	346 ± 3	14.5
Al-5251 (H22)	1.5	182 ± 1	212 ± 2	13
	2.5	179 ± 1	197 ± 1	11

2.2 Manufacturing of TWBs using EBW and LBW techniques

The TWBs were manufactured using both EBW and LBW techniques. Initial trials were carried out to optimise parameters for welding Al-5251 (H22) and Al-6082 (T6) sheets together. For this study, small off cuts were welded together and then pull tests were carried out to check if failure occurs at or away from the weld and to check elongation for each weld condition. Based on the results optimised weld

parameters for the manufacture of TWBs were determined. Table 3 shows the EBW optimised process parameters for full-scale trials. Total 9 samples (N1 – N9) were welded together with varying beam current (12 – 31 mA), beam speed (20 – 25 mm/s) and working pressure (3.6 – 9 × 10^{-4} mbar).

Table 3: Electron beam welding process parameters for manufacturing full scale TWBs

Sample No	Electron beam welding (EBW) parameters						
	Material-A	**Thickness-A (mm)**	**Material-B**	**Thickness-B (mm)**	**Beam current (mA)**	**Speed (m/min)**	**Working pressure (mbar)**
N1	Al-6082	1.5	Al-6082	1.5	16	1.5	5.3 × 10^{-4}
N2	Al-6082	1.5	Al-5251	1.5	14	1.5	5.3 × 10^{-4}
N3	Al-6082	1.5	Al-6082	2.5	18	1.2	5.3 × 10^{-4}
N4	Al-6082	1.5	Al-5251	2.5	19	1.5	4.6 × 10^{-4}
N5	Al-5251	1.5	Al-5251	1.5	12	1.2	4.1 × 10^{-4}
N6	Al-5251	1.5	Al-5251	2.5	18	1.5	4.1 × 10^{-4}
N7	Al-5251	1.5	Al-6082	2.5	18	1.5	4.1 × 10^{-4}
N8	Al-6082	2.5	Al-6082	2.5	31	1.5	9 × 10^{-4}
N9	Al-5251	2.5	Al-5251	2.5	26	1.2	3.6 × 10^{-4}

Table 4 shows the LBW optimised process parameters for full scale TWB trials. Total 9 samples (M1 – M9) were welded with varying focus of laser beam, laser power (2.8 – 4.3 kW) and speed (maintained at 3 m/min for all trials). The F=0 indicates when the centre of laser beam coincides with the centre of the weld seam and any other F values show deviations from that. These deviations were used in order to achieve the optimum weld quality. Figure 1 shows the net heat input for all the different weld conditions for TWBs (N1 – N9 and M1 – M9) manufactured with the EBW and the LBW. Equation 1 and Equation 2 show the net heat input calculation for both processes [26]. A higher net heat input can be seen for the LBW TWBs compared to their EBW counterparts and particularly ~33 – 42% higher net heat input is noticed for the dissimilar welds from the LBW process. The only exception to this is M9 condition, which shows ~5% lower heat input than N9 condition. Figure 2 shows two representative images of full scale TWBs (300 mm × 300 mm final dimension) and magnified images of weld beads manufactured by both EBW and LBW techniques. As can be seen from the image that the attempt was made to produce near identical levels of weld qualities from the two different processes.

Table 4: Laser beam welding process parameters for manufacturing full scale TWBs

Sample No	Laser beam welding (LBW) parameters						
	Material-A	**Thickness-A (mm)**	**Material-B**	**Thickness-B (mm)**	**Focus**	**Power (kW)**	**Speed (m/min)**
M1	Al-6082	1.5	Al-6082	1.5	F+3	2.8	3.0
M2	Al-6082	1.5	Al-5251	1.5	F+3	2.8	3.0
M3	Al-6082	1.5	Al-6082	2.5	F=0	3.8	3.0
M4	Al-6082	1.5	Al-5251	2.5	F=0	3.4	3.0

M5	Al-5251	1.5	Al-5251	1.5	F+5	2.8	3.0
M6	Al-5251	1.5	Al-5251	2.5	F=0	3.4	3.0
M7	Al-5251	1.5	Al-6082	2.5	F=0	3.7	3.0
M8	Al-6082	2.5	Al-6082	2.5	F=0	4.3	3.0
M9	Al-5251	2.5	Al-5251	2.5	F+5	3.7	3.0

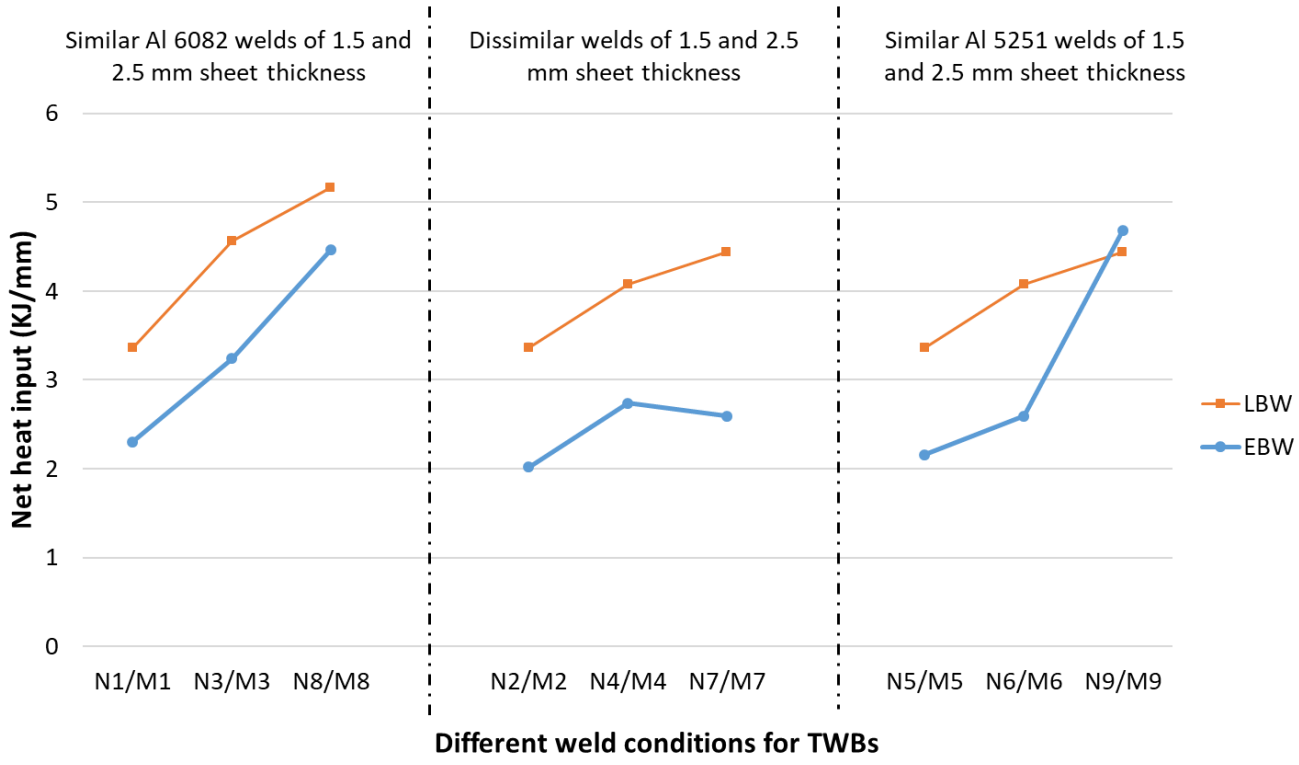

Figure 1: Net heat input of all different weld conditions for TWBs during both EBW and LBW processes

Equation 1: Net heat input for EBW [26]

Net heat input for EBW = $\frac{60VI}{1000v}$ where V is the voltage used (kV), I is the adjusted current (mA), v is the travel speed (mm/s)

Equation 2: Net heat input for LBW [26]

Net heat input for LBW = $\frac{60W}{v}$ where W is the laser power (kW), v is the travel speed (mm/s)

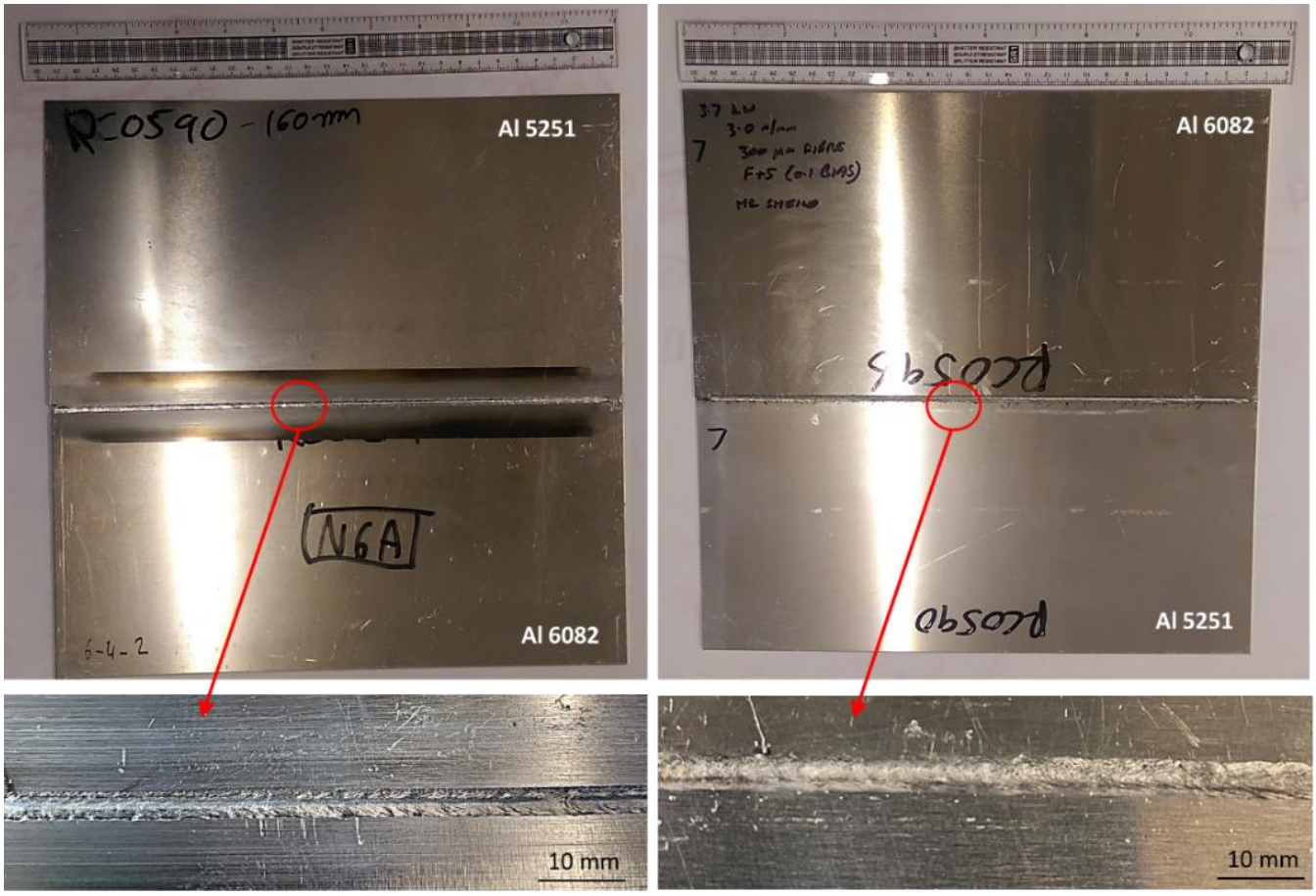

Figure 2: Representative images of the full scale TWBs (300 mm × 300 mm) and high magnification images of the welds manufactured using (a) EBW and (b) LBW techniques

2.3 Heat-treatment and stamping of TWBs

Figure 3 (a-d) shows all four components, made from H13 tool steel, of the tool assembly used in the current work for the stamping operation. The tool assembly, installed on a 500T hydraulic press at Advanced Forming Research Centre (AFRC) (see Figure 4), consists of a lower forming die housing (Figure 3a), a die insert with concaved cruciform impression (Figure 3b) that sits in the lower die housing, a locking/ejector plate (Figure 3c) that goes on the top of the lower die, and an upper die block with convexed cruciform impression and guide pillars that moves downwards to form the TWB locked between the plate (Figure 3c) and lower die assembly (Figure 3a and b).

Initially, stamping of the welded TWBs was trialled on the 500T press in as-received condition (hereafter named as 'M1- asR', 'N1-asR') i.e. without any PWHT. This led to severe cracking at the weld as well as in the parent sheet irrespective of the welding techniques used for manufacture of the TWBs. Moreover, LBW TWBs showed relatively more cracks than that in the case of EBW TWBs.

Figure 5 shows two such representative images for both EBW and LBW TWBs, where severe through thickness cracking occurred in the stamped parts as indicated. A downward velocity, of the top die, of 6 mm/s on the 500T hydraulic press resulted in localised thinning and cracking, whereas reducing the velocity to 3 mm/s provided better formability although with lesser cracks resulting in the formed parts. The cracking observed at the weld and in the parent material can be attributed to various factors including residual stresses generated due to both the EBW and the LBW processes as well as the variation in properties between the two materials used in the current work. Significant residual stresses have been reported for 6000 series aluminium alloys for both the EBW [27] and the LBW [28] processes. Moreover, the H22 condition for the Al-5251 and the T6 condition for the Al-6082 are tempers that impart high strength in these alloys whilst making them less formable.

The non-heat treatable alloy Al-5251 (H22) has reasonable formability and it is ideal for moderate bending with a good strength requirement in the final part [29], [30]. When substantially higher mechanical properties are required with minimal forming, the use of Al-6082 (T6) is typically recommended [30]. Aginagalde et al. [31] showed the effect of different heat-treatments on the formability of 1.5 mm thick Al-6082 sheet. They observed increased formability of Al-6082 sheet in O condition (415°C for 1 hour, followed by a cooling rate of 28°C/hour until 260°C) compared to the T6 condition (solution treated and artificially aged) due to presence of larger size precipitates concentrated at the grain boundaries in the latter. The T6 treatment (Solution treated up to 540°C for 2 hours followed by fast cooling and then 1.5 hours aging at 180°C) resulted in high strength in the final component but showed with significant geometrical distortions and large deformations due to bending.

Based on information available in literature a couple of annealing temperatures, 250^{o}C and 450^{o}C, were trialled to find out suitability for subsequent stamping. It was found that annealing at 450°C for 30 minutes followed by air cooling imparted adequate ductility for subsequent stamping operation of TWBs without any cracking at the weld and in the parent materials. Hence, all similar and dissimilar TWBs were heat-treated at 450°C for 30 minutes and subsequently full-scale stamping trials were performed for all 18 sample conditions (N1 – N9 and M1 – M9 as detailed in Table 3 and Table 4). Drawsol 850 was used as lubricant for stamping operation. For each sample condition, the stamping trials were successfully conducted at 0°, 0° with offset and 90° of the weld line alignment. All the heat-treated and stamped TWB parts (hereafter named as ‘M1-450°C’, ‘N1-450°C’ etc.) were then waterjet cut, for removal of excess edges, to their final shape. Figure 6 shows representative images of jet-cut, heat-treated and stamped TWB parts for different sample conditions, such as M3-450°C, M4-450°C, M8-450°C and N5-450°C.

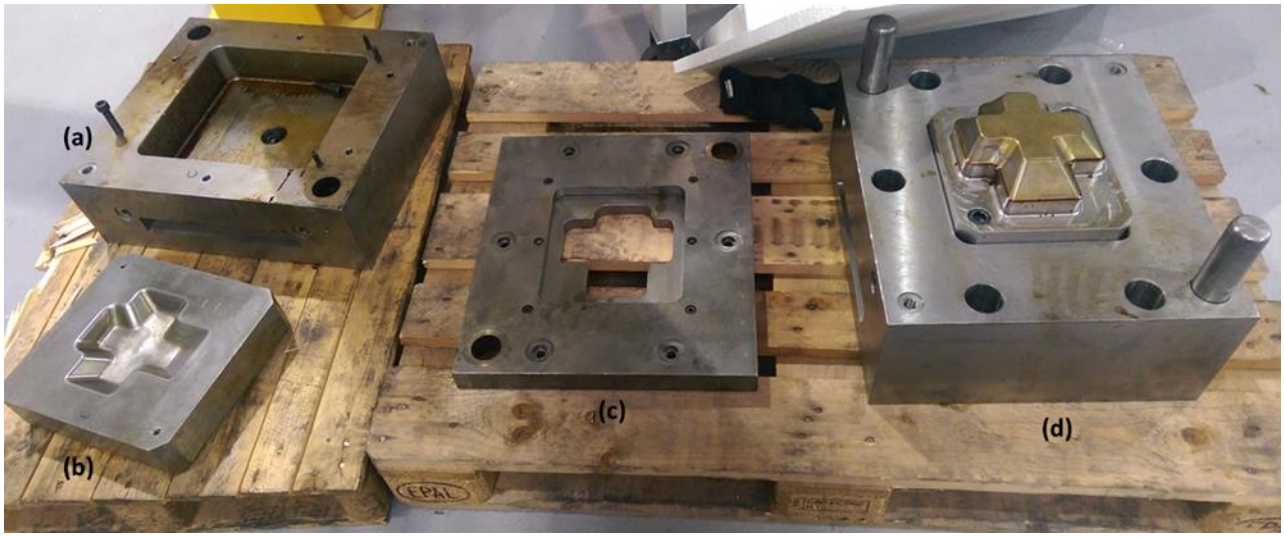

Figure 3: All components of tool assembly for the stamping operation – (a) lower forming die, (b) plus shaped impression that sits in the lower die block cavity, (c) stopper/ejector plate that goes on the top of the lower die, (d) upper die block with guide pillars that moves downward to press on the lower die assembly to form the stamped part.

(a)

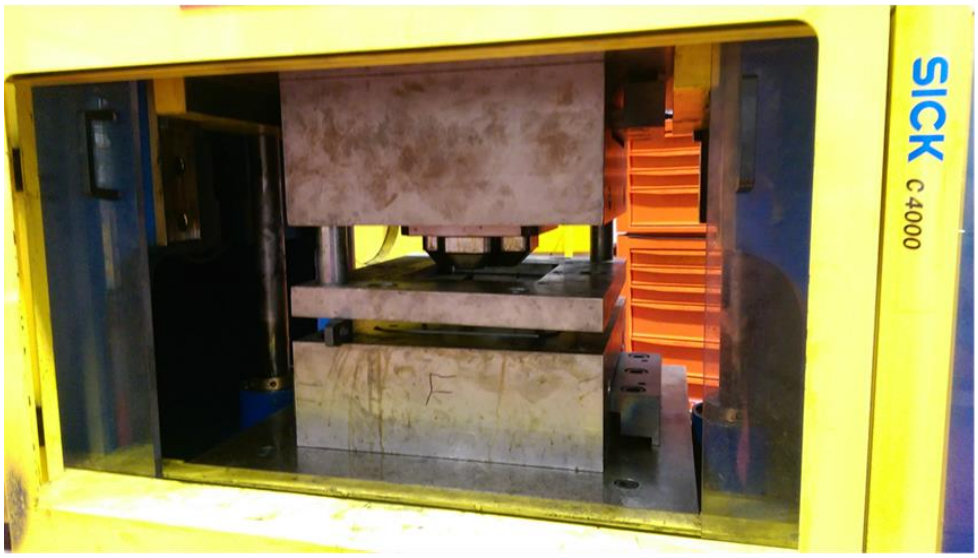

(b)

Figure 4: (a) AFRC's 500T hydraulic press and (b) a magnified view of the stamping tool assembly within 500T press

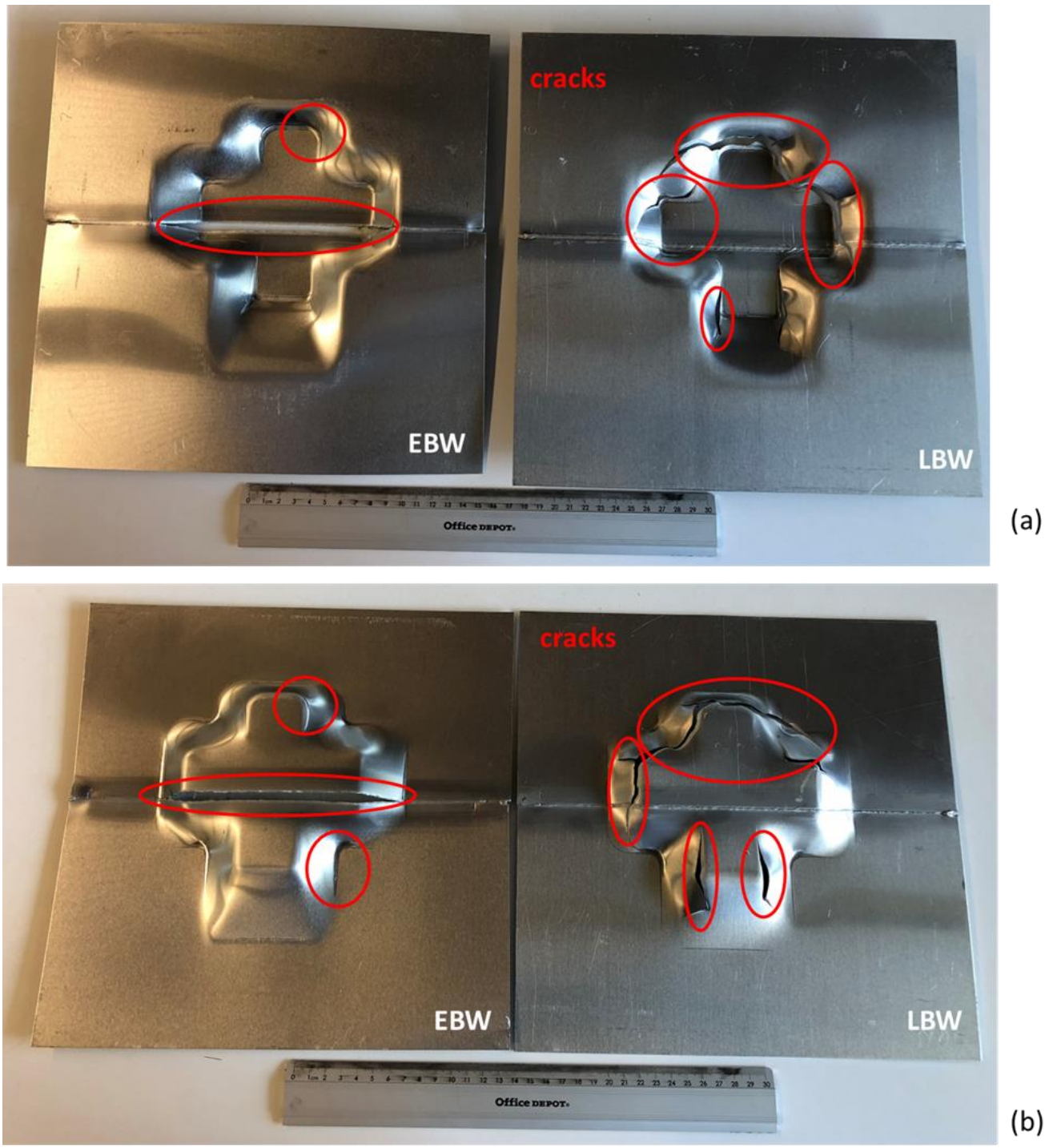

Figure 5: Representative images showing severe cracking, marked by red circles, observed at the weld and in the parent material in the stamped TWBs without any PWHT – (a) top or front side view and (b) back side view.

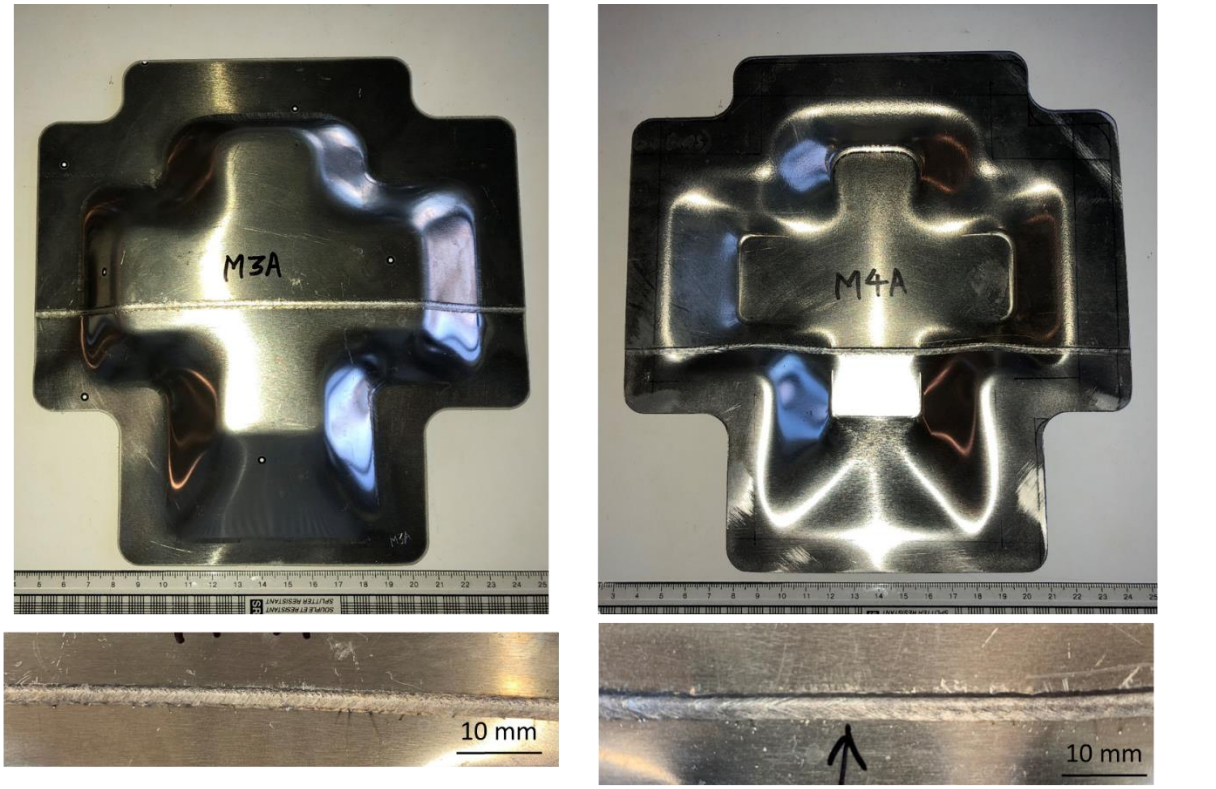

(a) M3-450°C : Al 6082 1.5 mm and 2.5 mm (LBW)

(b) M4-450°C : Al 6082 1.5 mm and Al5251 2.5 mm (LBW)

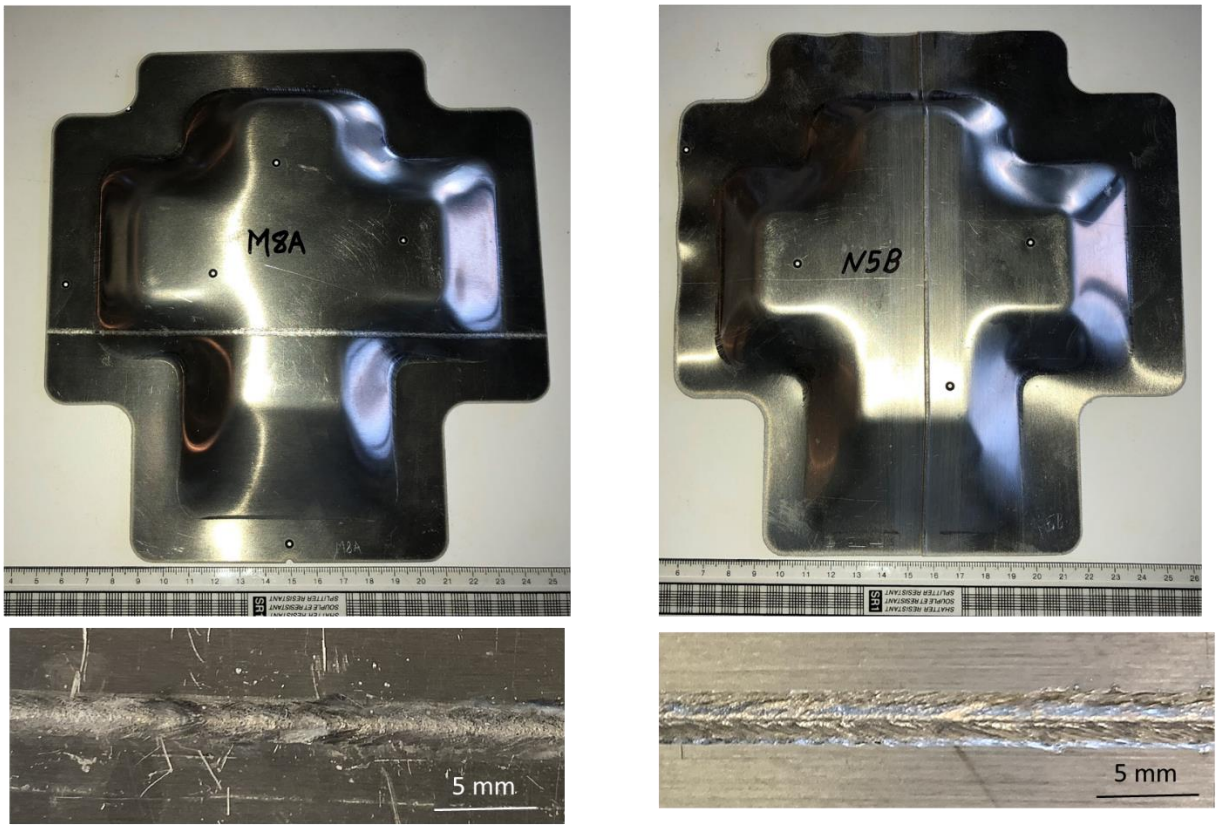

(c) M8-450°C : Al 6082 2.5 mm and 2.5 mm (LBW)

(d) N5-450°C : Al 5251 1.5 mm and 1.5 mm (EBW)

Figure 6: Representative images of post-weld heat treated, stamped and waterjet cut TWB parts for different sample conditions – (a) M3-450°C, (b) M4-450°C, (c) M8-450°C and (d) N5-450°C. Note that the stamping trials have been at 0°, 0° with offset and 90° of the weld line alignment.

3. Experimental details

Table 5 summarises the measurements and analysis performed on selected EBW and LBW TWBs before and after the stamping operation. A GOM ATOS TripleScan III system was used, a non-contact optical metrology system, for scanning the stamped TWBs to generate 3D model of the part. This equipment is capable of digitizing various geometries into a CAD representation of the actual by using blue light technology. This is an effective way of generating 3D model of the formed component with a dimensional measurement accuracy of up to 30 – 35 microns. This enables measuring thickness variations across the final formed part surfaces and helps to decide if the formed part meets the dimensional and thickness variation requirements for a specific application. In this study, the EBW and LBW 'asR' and '450°C' TWBs for GOM measurement (as detailed in Table 5) were selected in such a way that covered both similar and dissimilar welds for the two different welding techniques.

Figure 7 shows a schematic of sample extraction scheme for pull test, microstructure and hardness tests from both sub-scale EBW and LBW parts before (i.e. asR) and after the PWHT (at 450°C). The pull test samples were 25 mm wide × 240 mm long, with a gauge length of 120 mm. The pull tests were performed in Zwick Z250 machine at ambient temperature and at 450°C for all EBW (N1 – N9) and LBW (M1 – M9) samples as detailed in Table 5. Each test was repeated three times for repeatability and the tests were performed at a strain rate of 0.005/s.

A Struers hardness tester was used for hardness measurement of all the EBW and LBW 'asR' and '450°C' samples according to ASTM standard E384 – 11 [32]. The indents were made in a rectangular matrix of 21 indents (3 rows × 7 columns) using a Vickers indenter with a fixed load of 0.2 kgf. Figure 8 shows images, produced from Struers hardness tester computer, of the resin mounted weld specimens with indents locations highlighted by blue diamonds on the schematics to the right. The images show two columns of indents placed on the parent materials on either side of the weld. One column of indents each was placed within the weld and on the HAZ at either side of the weld (regions marked with the white dotted lines). The distance between any two indents along X direction was kept fixed at 2 mm, whereas along Y direction, it was set as 0.5 mm for sheet thickness of 1.5 mm (Figure 8a) and 1 mm for sheet thicknesses of 2.5 mm (Figure 8b) respectively. For welding of sheets with different thicknesses, the same indent distribution for sheet thickness of 1.5 mm was followed.

Likewise, the microstructural analysis was done on all the EBW and LBW 'asR' and '450°C' samples using a FEI Quanta FEG 250 – SEM. All these samples were mounted in the conductive resin moulds followed by grinding with P800 and P1200 SiC abrasive grit papers and polishing with 9µm UltraPol,

3µm Trident and Microcloth with 0.02µm colloidal silica suspension followed by 2 – 3 hours of vibro-polishing at 50% amplitude. The SEM images were collected using backscattered mode for a better image contrast.

Table 5: Summary of measurements and analysis performed on EBW and LBW TWBs before and after stamping

Samples	Measurement and analysis			
	GOM	Pull tests	Hardness	Microstructure
asR EBW TWBs	–	N1 – N9		–
asR LBW TWBs	–	M1 – M9		selected
heat-treated (450°C) and stamped EBW TWB parts	N5-450°C, N7-450°C and N9-450°C	N1 – N9		
heat-treated (450°C) and stamped LBW TWB parts	M1-450°C, M3-450°C and M8-450°C	M1 – M9		

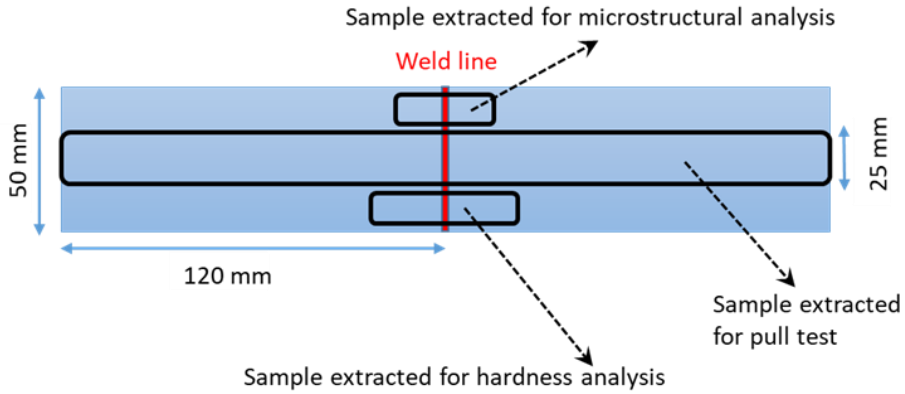

Figure 7: Schematic of sample extraction (for pull tests, microstructure and hardness tests) from both sub-scale EBW and LBW TWBs before (i.e. asR) and after heat-treatment (at 450°C).

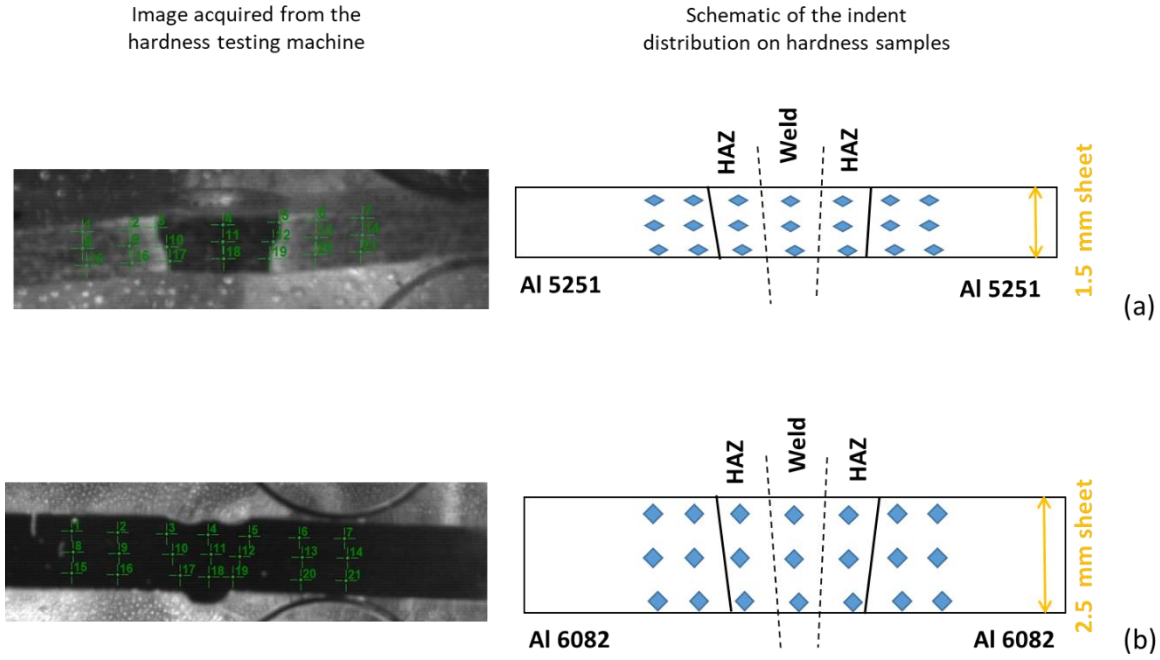

Figure 8: Schematic of the indent distribution (marked with blue) on representative samples for hardness measurement – (a) M1 with 1.5 mm sheet thickness and (b) M9 with 2.5 mm sheet thickness

4. Results and discussion

4.1 Mechanical properties of TWBs

Figure 9 and Figure 10 show load (kN) versus displacement (mm) behaviour analysed from pull tests conducted on all the EBW and the LBW samples, respectively, in both the asR and after the PWHT conditions. The dotted and solid lines are used to represent the load vs displacement behaviour of asR and heat-treated samples respectively. In general, all the heat-treated samples exhibit considerably lower peak load compared to their asR counterparts due to PWHT causing softening of the weld and the parent sections. This can be attributed to annealing effect imparted by the heat treatment especially to the Al-5251 and to over-aging in Al-6082. As reported by Aginagalde et al. [31], heat treatments on Al-6082 around 415^{o}C and especially below 540^{o}C result in no phase changes however over-aging occurs with increase in mass fraction of precipitates and coalescence of small precipitates into large particles as a result. In addition to the significant drop in peak load, the welds after PWHT also exhibit marked improvement in displacement or elongation at failure with the exception of N2 and N6 samples (Figure 9). The improvement in elongation is more noticeable in case of the LBW samples compared to their EBW counterparts, although the peak load drop is similar in both types of welds. Except M8 (Figure 10), all LBW welds fail at a significantly higher displacement after PWHT. It is noteworthy that the LBW samples consistently have higher heat input (see Figure 1), compared to their EBW counterparts. This appears to have affected the elongation of the LBW samples after the PWHT by causing marked improvement in the same. The combination of significant softening, indicated by drop in the peak load, and improved elongation is believed to have contributed to the much improved formability of both types of TWBs after PWHT.

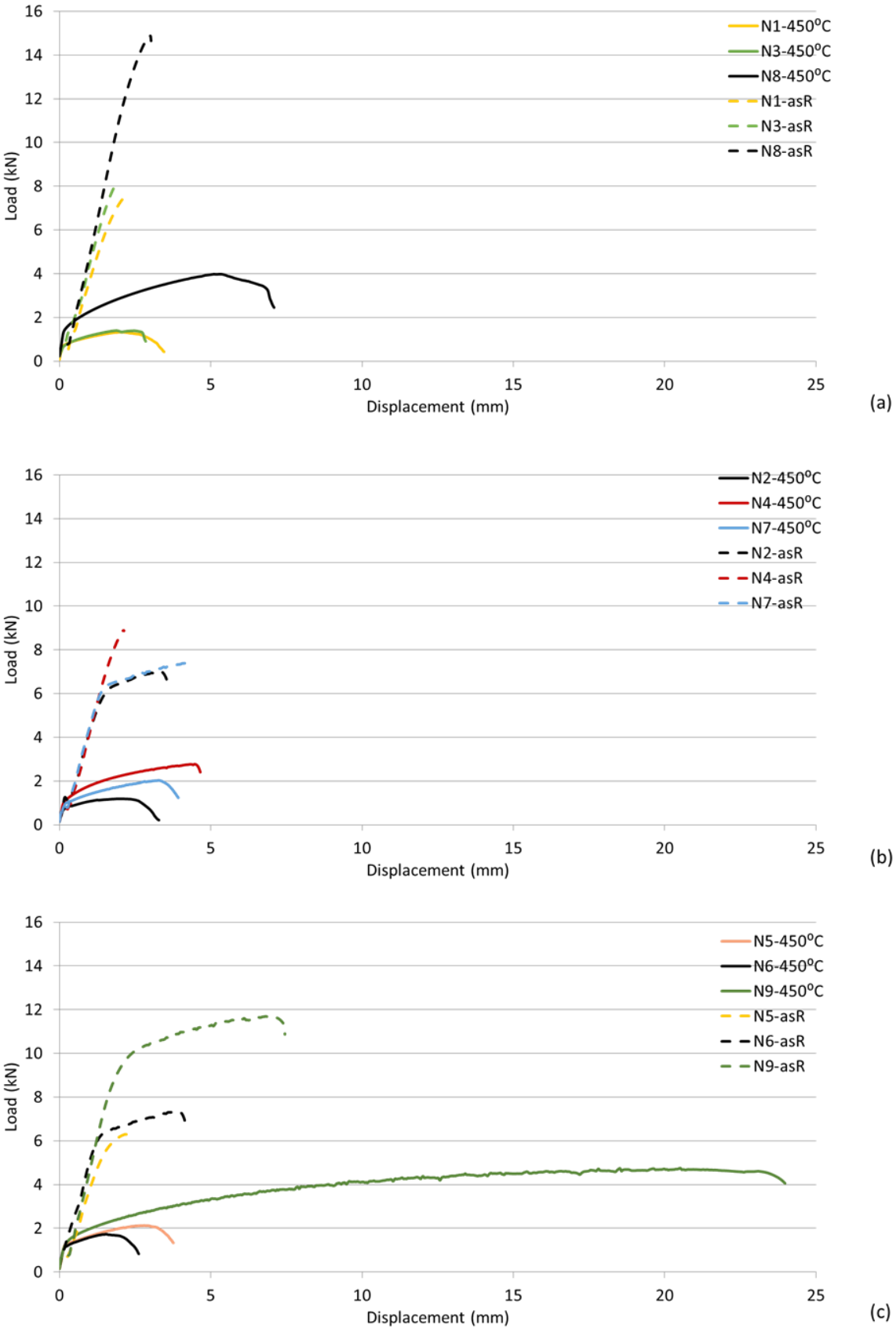

Figure 9: Load vs displacement behaviour of EBW TWBs – (a) similar Al-6082 welds, (b) dissimilar welds, and (c) similar Al-5251 welds

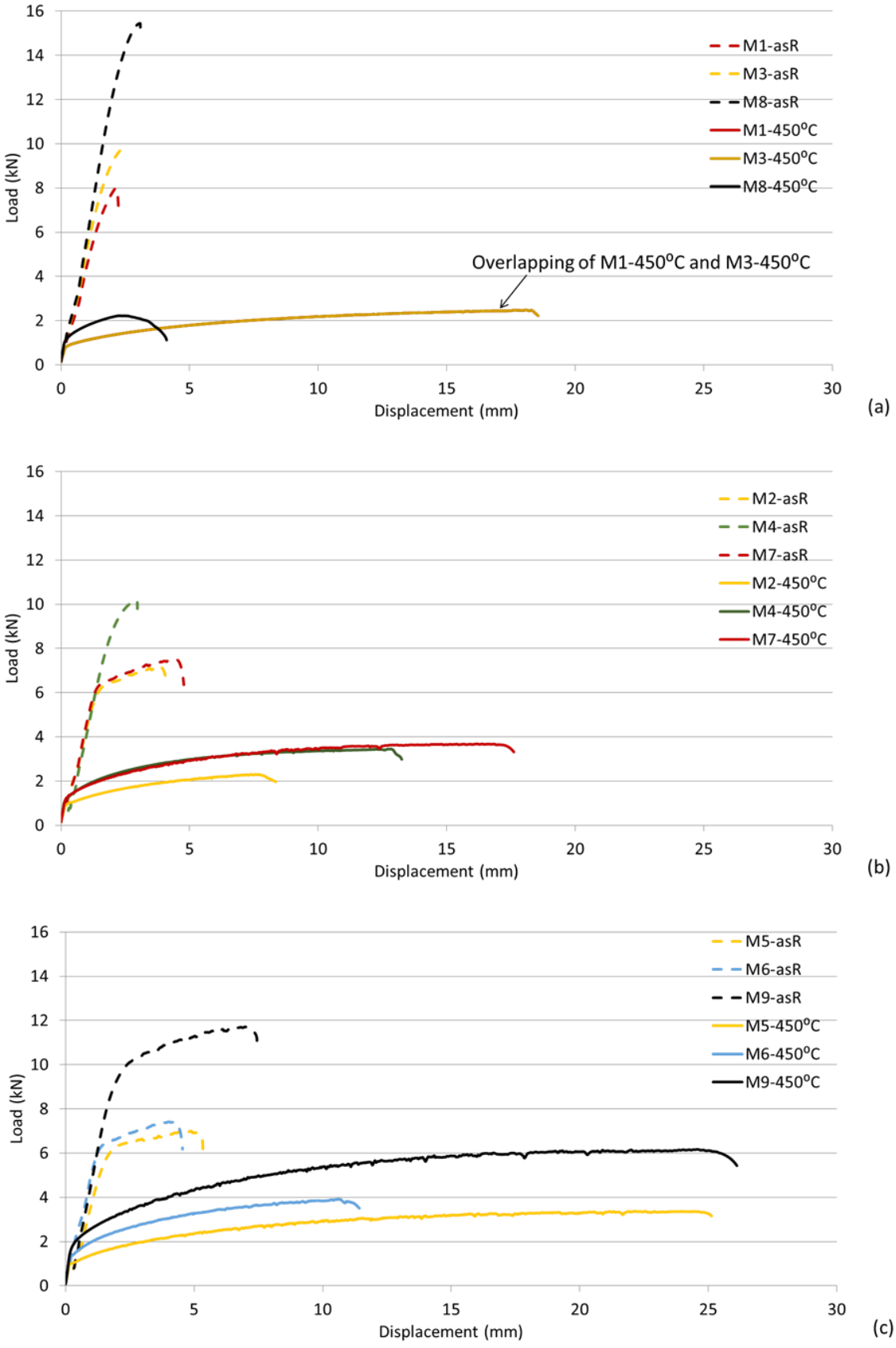

Figure 10: Load vs displacement behaviour of LBW TWBs – (a) similar Al-6082 welds, (b) dissimilar welds, and (c) similar Al-5251 welds

4.2 Hardness of TWBs

4.2.1 Hardness distribution of EBW TWBs

Figure 11, Figure 12 and Figure 13 show the hardness distribution of EBW TWBs for similar Al-6082 welds, similar Al-5251 welds and dissimilar welds respectively for both asR and heat-treated conditions. The hardness scale range is kept in the range of 40 – 100 HV to have a comparable view of all welded samples. Amongst the similar Al-6082 welds (Figure 11), the hardness distribution is significantly varied in asR condition from the weld zone to the parent material (60 – 100 HV) with minimum hardness observed either in the weld or in the HAZ. The PWHT reduces the hardness down to a much narrower range, of 40 – 56 HV, leading to a homogenous hardness distribution throughout the weld zones of the TWBs. On the other hand, the similar Al-5251 welds (Figure 12) show slight variation in the hardness distribution from the weld zone to the parent material (40 – 67 HV), for the asR condition, and this is reduced to a slightly narrower range (40 – 52 HV) after the heat-treatment. For the dissimilar welds (Figure 13), a wider range in the hardness distribution (57 – 100 HV) is observed throughout the asR condition which is significantly reduced to a much narrower range (40 – 51 HV) after the heat treatment.

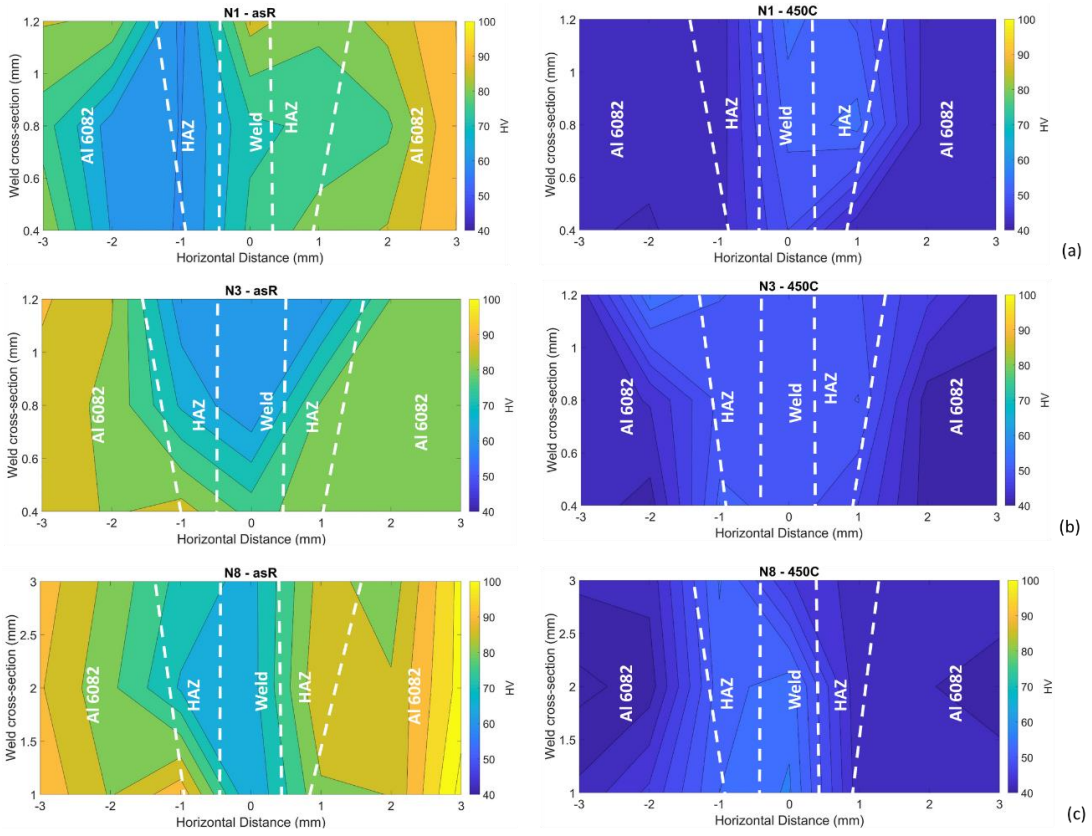

Figure 11: Hardness distribution of EBW TWBs for similar Al-6082 welds at both asR and heat-treated (450ºC) conditions – (a) N1, (b) N3, and (c) N8

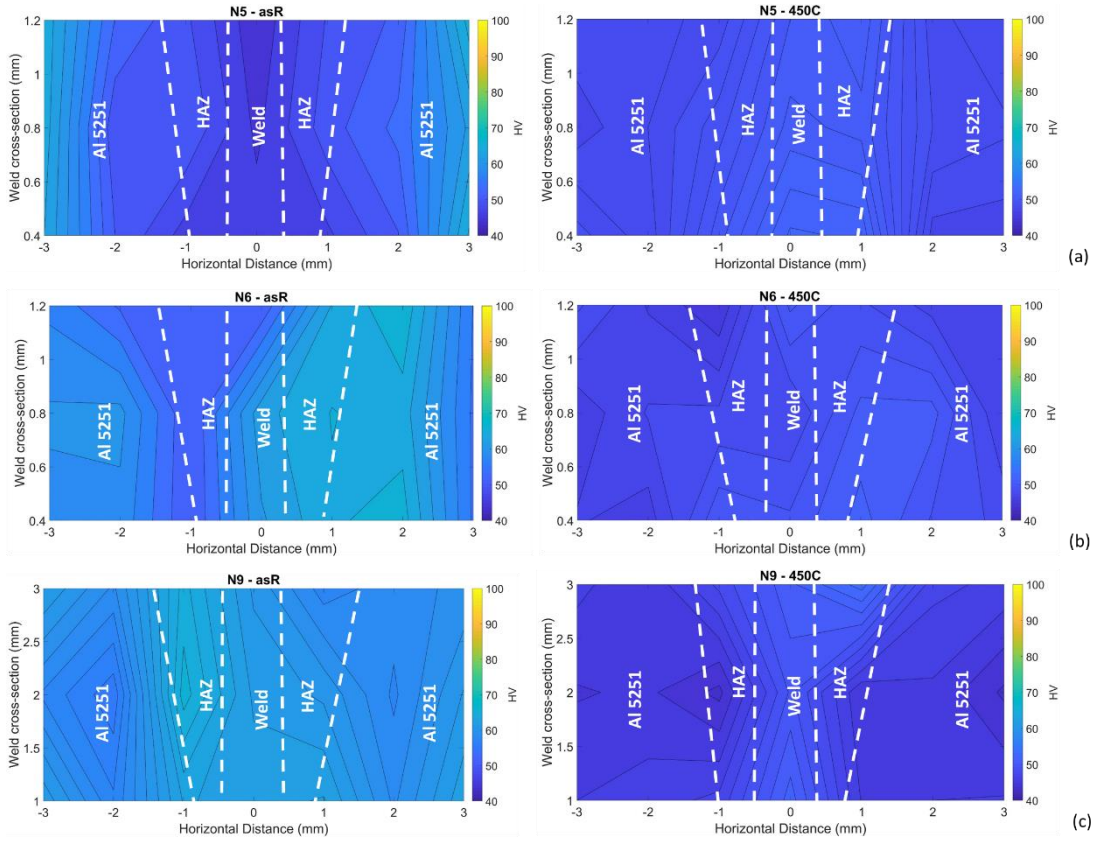

Figure 12: Hardness distribution of EBW TWBs for similar Al-5251 welds at both asR and heat-treated (450ºC) conditions – (a) N5, (b) N6, and (c) N9

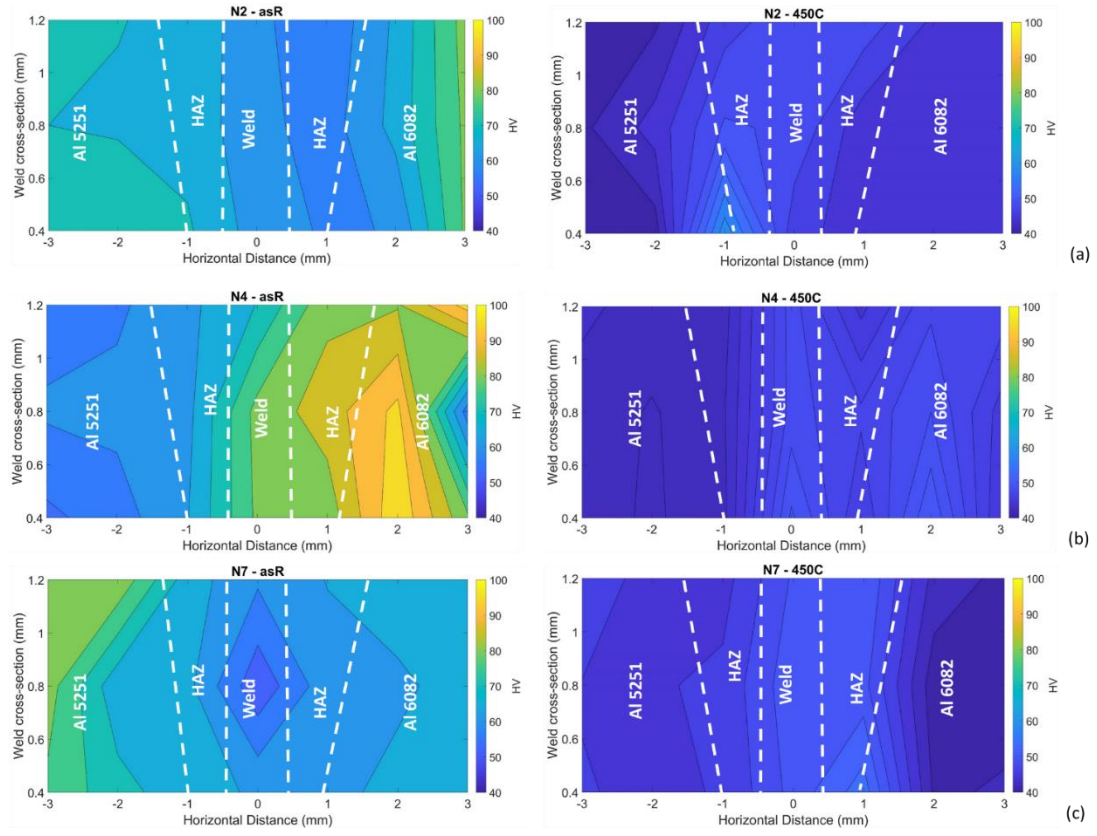

Figure 13: Hardness distribution of EBW TWBs for dissimilar welds at both asR and heat-treated (450ºC) conditions – (a) N2, (b) N4, and (c) N7

4.2.2 Hardness distribution of LBW TWBs

Figure 14, Figure 15 and Figure 16 shows the hardness distribution of LBW TWBs for similar Al-6082 welds, similar Al-5251 welds and dissimilar welds respectively for both asR and heat-treated conditions. Amongst the similar Al-6082 welds (Figure 14), the hardness ranged from 56 to 90 HV for the asR condition with lower hardness in the weld and the HAZ compared to that for the parent. Similar to the EBW TWBs, the PWHT reduced the hardness variation to a homogenous hardness distribution (40 – 55 HV) throughout the TWBs. For the similar Al-5251 welds (Figure 15), a relatively narrower variation the hardness (40 – 70 HV) is observed from the weld zone to the parent material for the asR condition which is further reduced (40 – 57 HV) following the PWHT. For the dissimilar welds (Figure 16), the hardness exhibits a smooth transition from the harder Al-6082 parent, through the weld zone, to the softer Al-5251 parent in the asR condition (55 – 90 HV). The PWHT eliminates this transition resulting in a more homogenous hardness distribution (40 – 52 HV) throughout the dissimilar TWBs with slightly higher hardness evident in the weld and the HAZ areas.

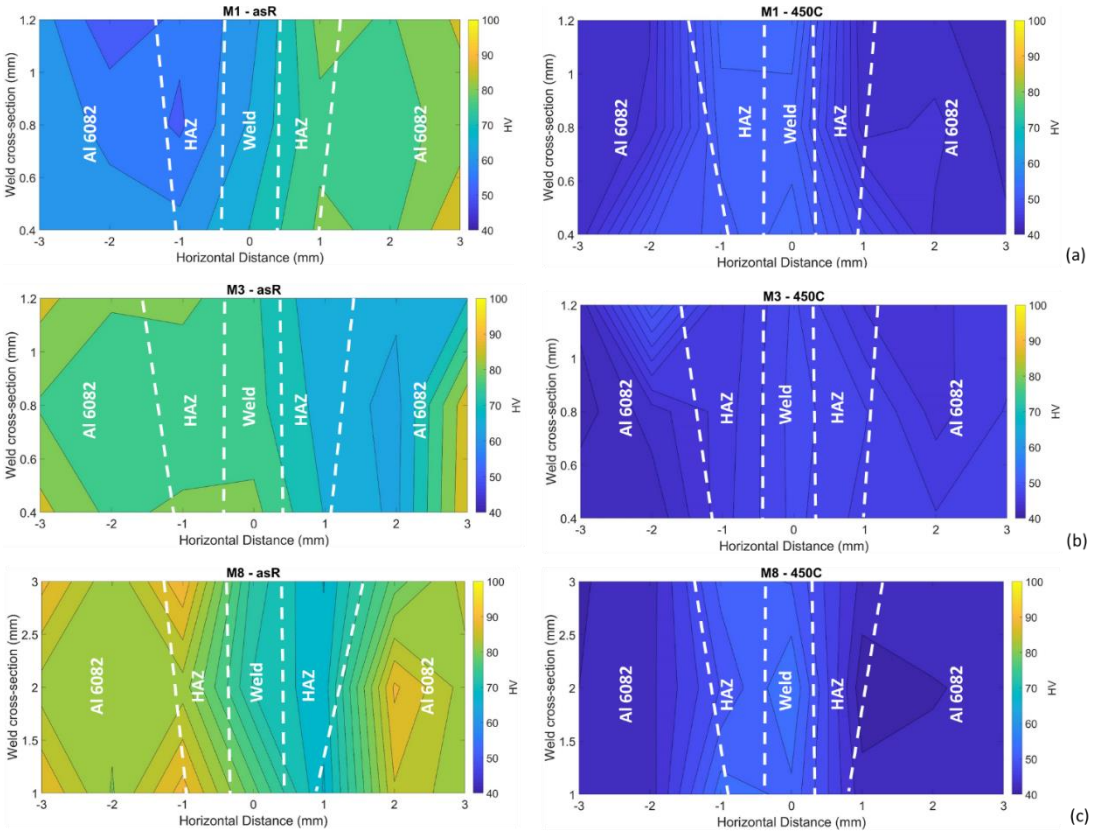

Figure 14: Hardness distribution of LBW TWBs for similar Al-6082 welds at both asR and heat-treated (450ºC) conditions – (a) M1, (b) M3, and (c) M8

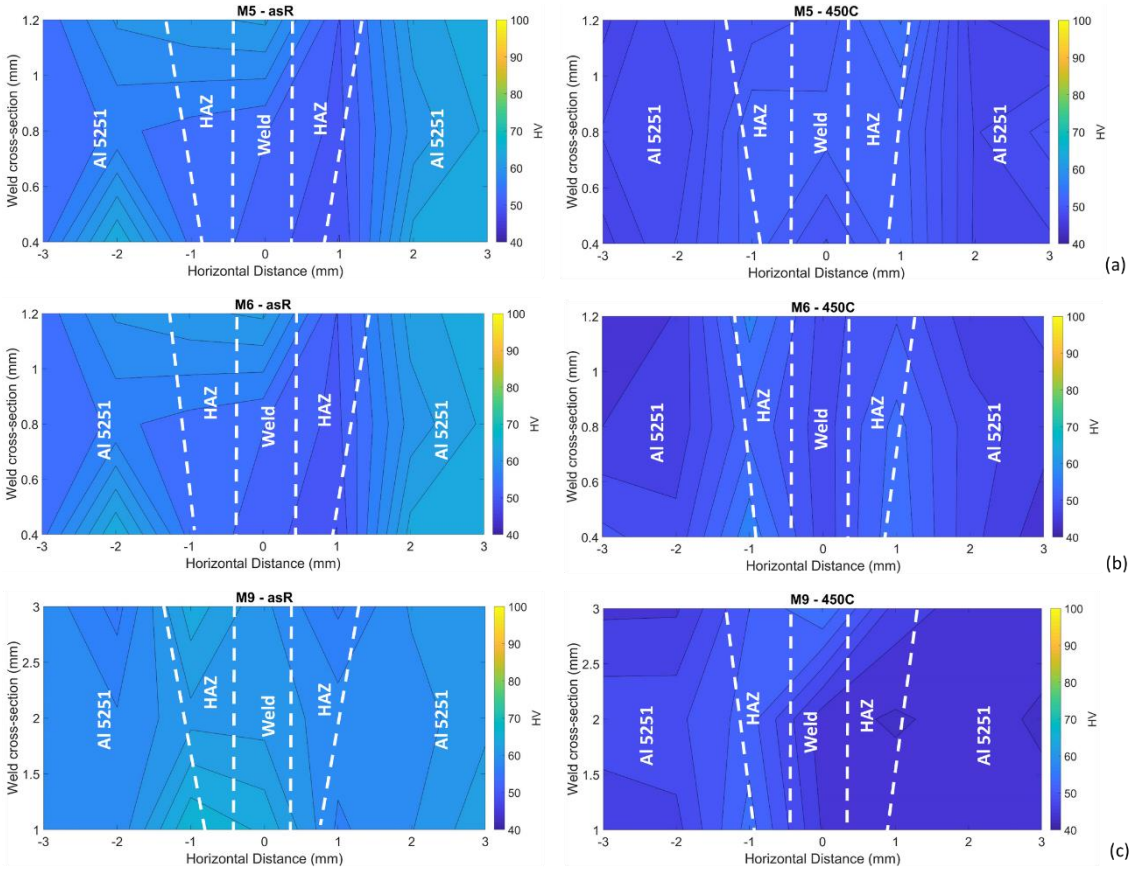

Figure 15: Hardness distribution of LBW TWBs for similar Al-5251 welds at both asR and heat-treated (450ºC) conditions – (a) M5, (b) M6, and (c) M9

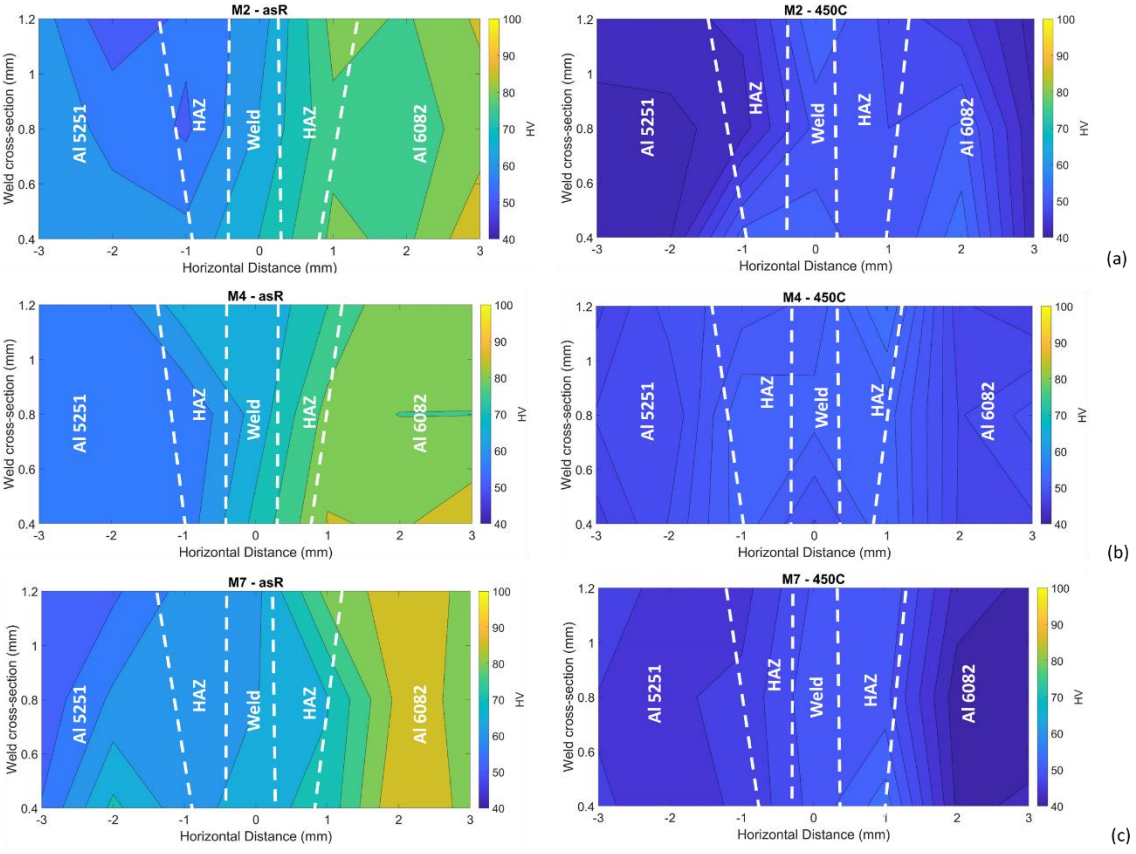

Figure 16: Hardness distribution of LBW TWBs for dissimilar welds at both asR and heat-treated (450ºC) conditions – (a) M2, (b) M4, and (c) M7

4.3 Microstructure analysis of LBW and EBW TWBs

SEM micrographs for LBW TWBs, in asR and PWHT conditions, are presented in Figure 17. Each micrograph contains montage of several individual micrographs to create a continuous micrograph across the weld covering the parent materials on either side with the welds in the middle. Before heat-treatment (i.e. asR condition), the M2 condition shows typical re-solidified structure with large equiaxed grains in the FZ, elongated grains in the HAZ and fine grains in the parent materials (Figure 17a). No significant changes in the overall weld microstructure can be seen in case of the PWHT micrograph, of the M2 condition, except formation of slightly refined grains in the FZ (Figure 17b). Similar microstructural features are observed for M4 condition before and after the PWHT (Figure 17c and Figure 17d respectively) with a reduced weld thickness as a result of the heat-treatment. The grain growth is noticed only for the parent Al-5251 of 2.5 mm thickness after PWHT. The M7 condition shows similar microstructural features as well as similar weld thickness before and after heat-treatment (Figure 17e and Figure 17f respectively). Although no phase change is expected at this temperature, however refinement and decreased mass percentage of Mg_2Si precipitation is anticipated based on the Al-Mg-Si phase diagram as discussed earlier in section 4.1.1. The presence of Mg_2Si particles can be seen as very fine bright particles dispersed, mainly on the Al-6082 side of the welds, due to low magnification of images. Figure 18 shows the magnified image of the encircled area in M7 – 450ºC (Figure 17f), which indicates presence of blocky Mg_2Si particles in the Al-6082 region and very fine Mg_2Si particles resulting from re-precipitation upon cooling of weld.

The objective of micrography in the current work is to cover a large area to make general observation about the grain structure in different zones and demonstrate weld quality which appears to be largely defect free from any cracking and any noticeable coarse porosity. Low magnification secondary electron mode SEM images are provided in Figure 19, for one of the LBW, M6, and the EBW, N9, samples after PWHT to demonstrate weld penetration between the two parent materials and absence of any cracks or any noticeable spherical coarse porosity. However, presence of fine porosity (of 10 microns or below) cannot be denied completely due to the nature of the welding processes employed in the current work. Moreover, metallographic preparation of aluminium alloys is challenging in that it is very likely to suffer from pick up of silica and other particles from diamond cloths which appear as dark spots, under backscattered mode, and especially are not spherical like typical porosity found in welds [33]. However, presence of these can confuse microstructure analysis. Since the porosity characterisation was not a key

objective for the present work, any in-depth analysis on porosity characterisation and quantitative analysis of grains or precipitates has not been conducted. The focus has mainly been on successful cold forming of the TWBs by imparting suitable PWHT.

Figure 20 shows the microstructure of heat-treated LBW TWBs around the weld zone for all similar Al-6082 welds. M1, M3 and M8 conditions show similar re-solidified structure with large equiaxed grains in the FZ, elongated grains in the HAZ and fine grains in the parent materials. Figure 20a shows formation of wider FZ and smaller HAZ when welding of 1.5 mm sheets in M1 condition. Exactly opposite behaviour, i.e. smaller FZ and wider HAZ, is observed while welding of 2.5 mm sheets in M8 condition (Figure 20c). Almost similar width of FZ and HAZ is observed for M3 condition, which represents welding between 1.5 mm and 2.5 mm sheets. (Figure 20b). Figure 21 shows the microstructure of welds of the PWHT LBW TWBs for all similar Al-5251 welds. M5, M6 and M9 conditions show re-solidified structure with large equiaxed grains in the FZ and considerably smaller elongated grains followed by very fine grains in the HAZ. Slightly wider FZ is observed in M6 as compared to M5 and M9. In M5 and M6, the parent Al-5251 of 1.5 mm thickness retains its fine grain structure even after PWHT (Figure 21a and Figure 21b respectively), whereas a clear grain growth is noticed for parent Al-5251 of 2.5 mm thickness in M6 and M9 (Figure 21b and Figure 21c respectively) as a result of the PWHT. It is noteworthy that despite quantifiable changes in the pull tests and the hardness results, no obvious microstructure changes can be observed between the asR and the PWHT cases. This can be attributed largely to static recovery which is characteristic softening mechanism in high stacking fault energy materials such as pure aluminium and its alloys [34]. The PWHT in the current work, therefore, acts as an effective stress relief treatment after welding and imparting softening through static recovery through annealing in Al-5251 and a combination of static recovery, increase in volume fraction of precipitates in Al-6082 (loss of strength due to over-aging).

Figure 22a shows the microstructure of heat-treated EBW TWBs around the weld zone for similar Al-6082 welds. It is noteworthy that due to absence of any marked differences between the asR and the PWHT microstructure, similar to that observed for the LBW TWBs, only the PWHT microstructure are presented in this section. The N1, N3 and N8 conditions contain large, elongated grains and fine grains within the HAZ and the parent materials respectively similar to their LBW counterparts (Figure 20). Figure 22b shows the microstructure of heat-treated EBW TWBs around the weld zone for dissimilar welds. N2 and N4 show microstructure very similar to their LBW counterparts (Figure 17). Figure 22c shows the microstructure of heat-treated EBW TWBs around the weld zone for similar Al-5251 welds and the microstructures of N5, N6 and N9 are observed very similar to their LBW counterparts (Figure 21). Similar to M4, M6 and M9, the grain growth is noticed in parent Al-5251 of 2.5 mm thickness in case of N4, N6 and N9 after annealing. Beside this, all EBW TWBs show slightly less tapered weld

zone compared to their LBW counterparts, but overall no significant difference in terms of weld microstructure (including any noticeable presence of coarse porosity and cracks). In addition to this, the high net heat input of LBW leads to higher average weld width (~2 – 2.6 µm) as compared to their EBW counterparts (~1.7 – 2.4 µm), however exception is noted for M3/N3 conditions.

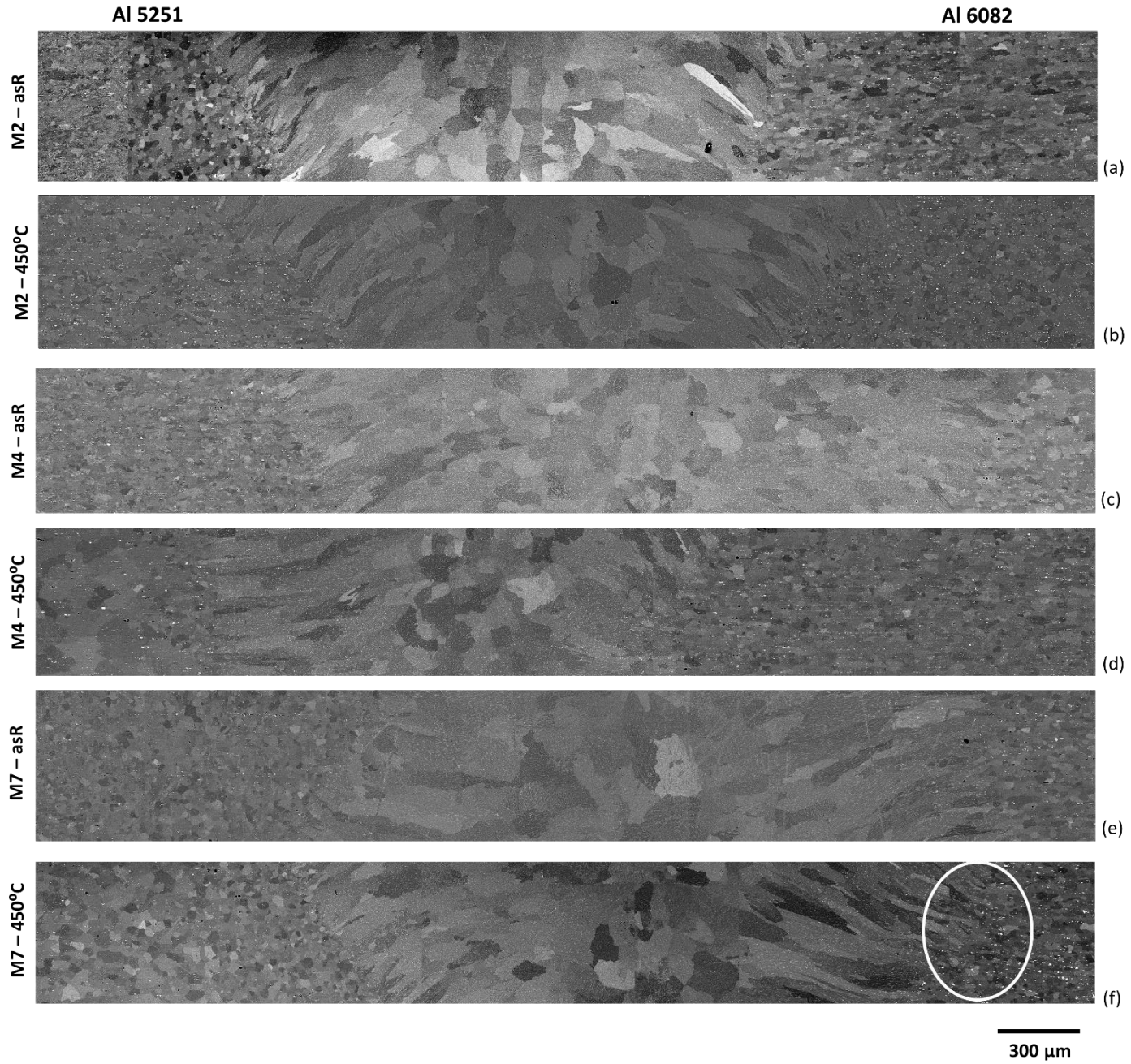

Figure 17: Microstructure of LBW TWBs around the weld zone for dissimilar welds – (a) M2- asR, (b) M2 – 450°C, (c) M4- asR, (d) M4 – 450°C, (e) M7- asR and (f) M7 – 450°C

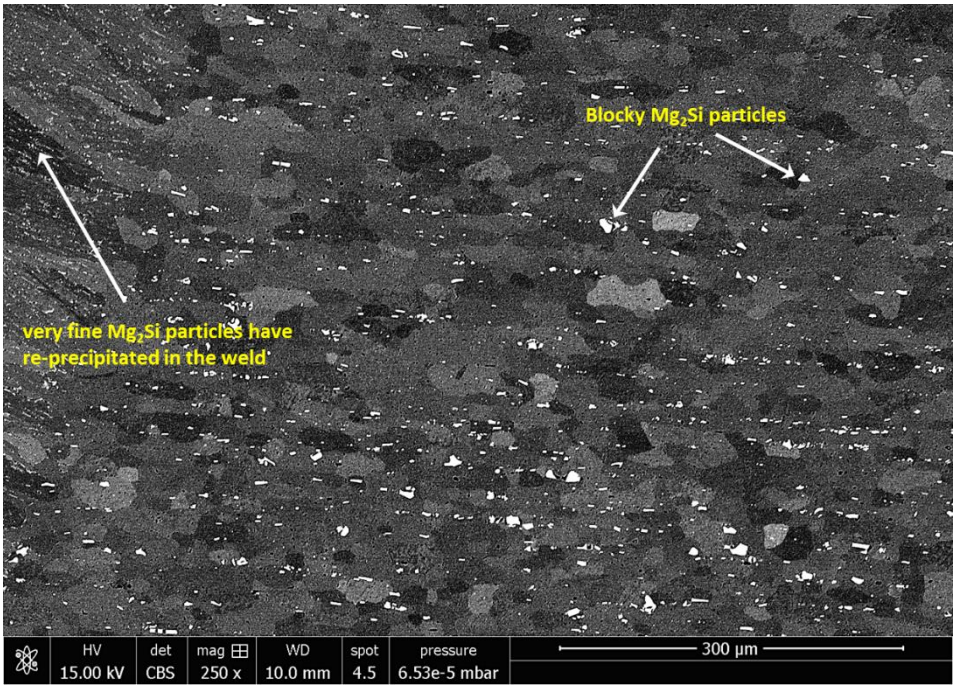

Figure 18: Magnified image of the encircled area in M7 – 450ºC (Figure 17f) showing presence of blocky Mg2Si particles in the Al-6082 region and very fine Mg2Si particles resulting from re-precipitation upon cooling of the weld

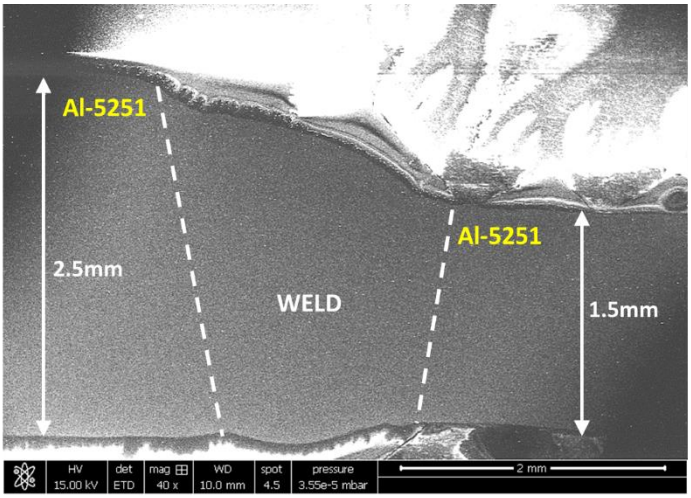

(a)

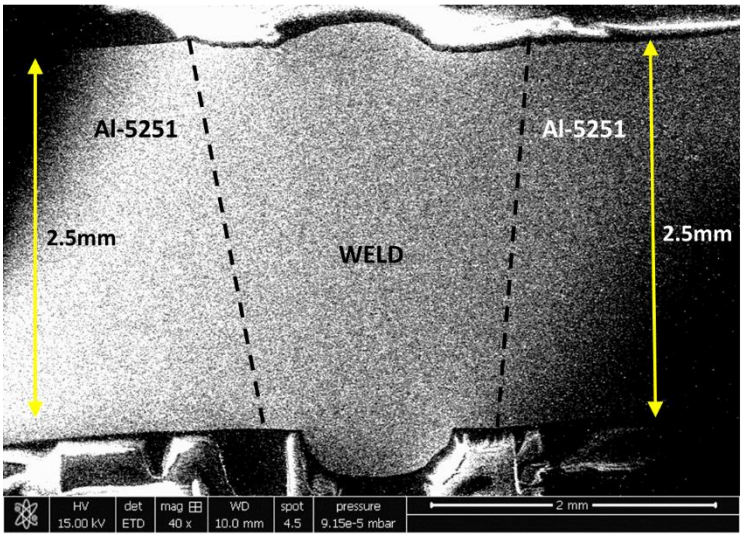

(b)

Figure 19: Low magnification SEM images showing weld penetration between the two parent materials for both LBW and EBW processes – (a) M6 – 450ºC and (b) N9 – 450ºC

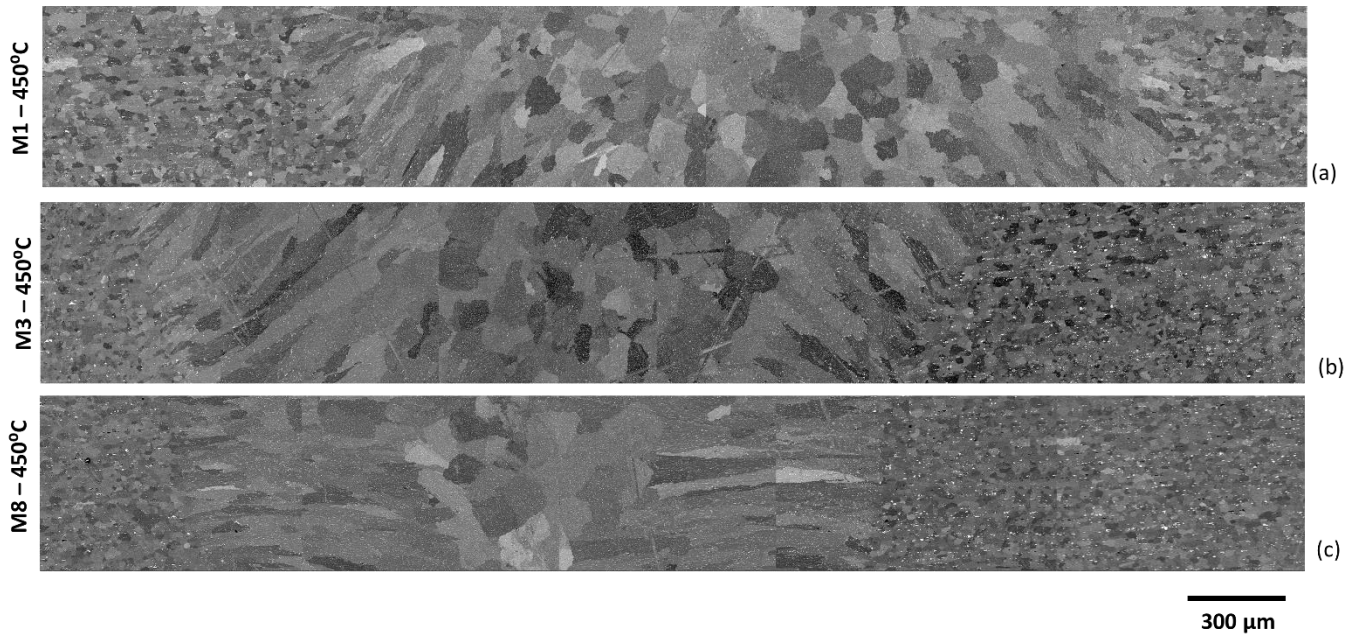

Figure 20: Microstructure of heat-treated LBW TWBs around the weld zone for similar Al-6082 welds – (a) M1 – 450ºC, (b) M3 – 450ºC, and (c) M8 – 450ºC

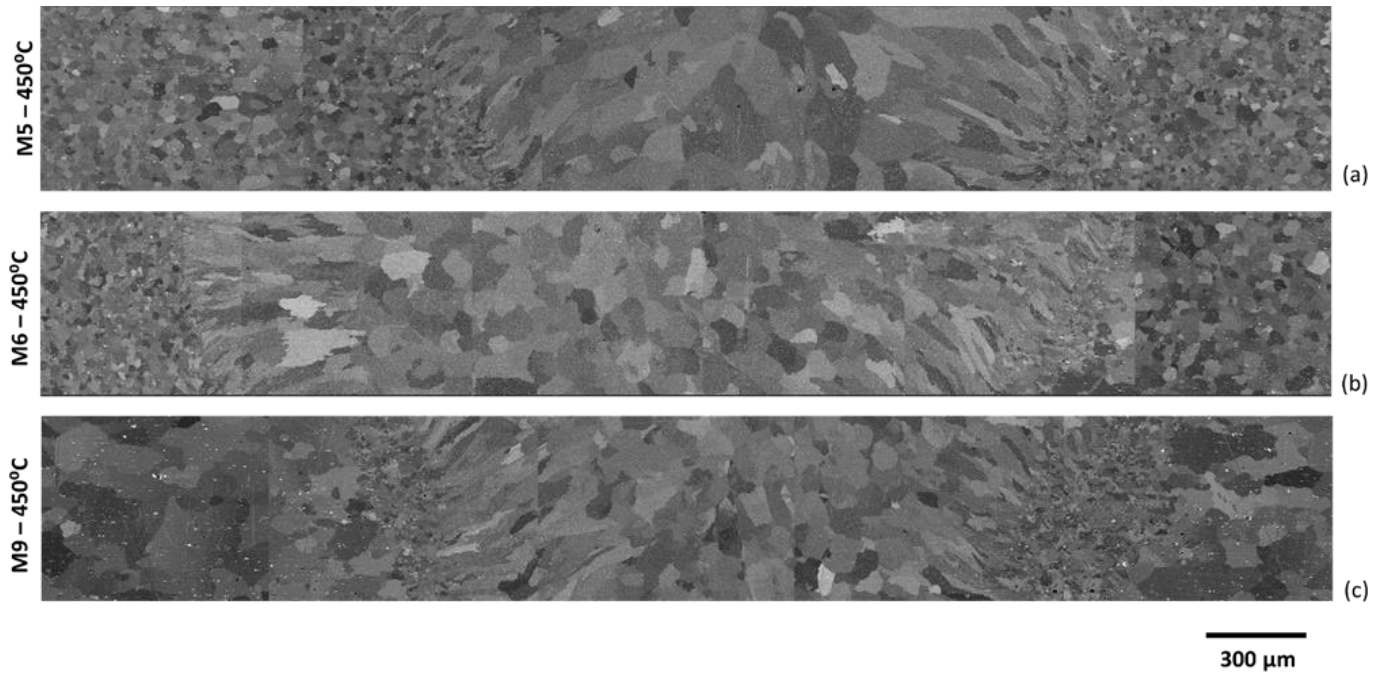

Figure 21: Microstructure of heat-treated LBW TWBs around the weld zone for similar Al-5251 welds – (a) M5 – 450ºC, (b) M6 – 450ºC, and (c) M9 – 450ºC

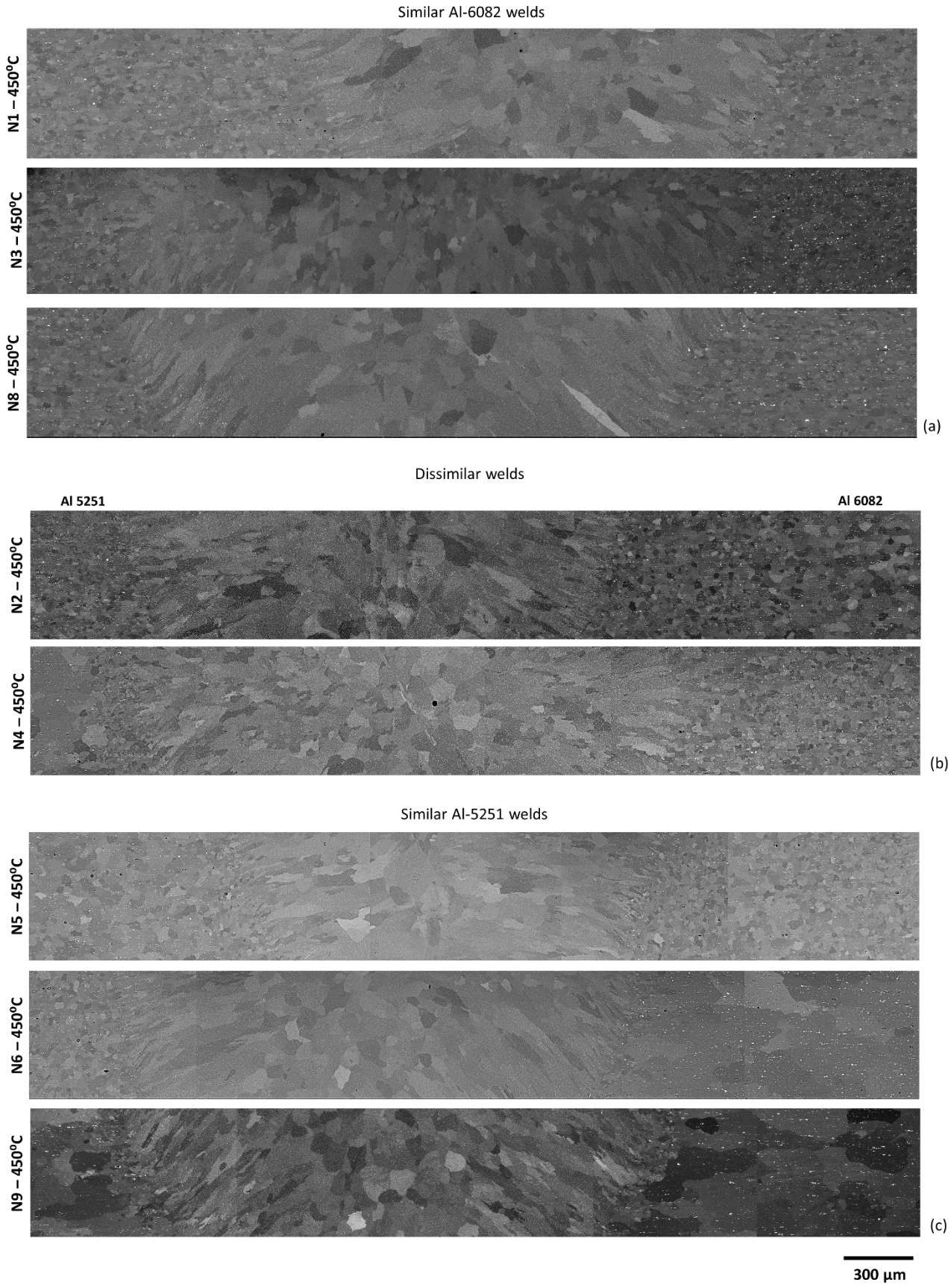

Figure 22: Microstructure of heat-treated EBW TWBs around the weld zone – (a) similar Al-6082 welds, (b) dissimilar welds, and (c) similar Al-l5251 welds

4.4 GOM Measurement of full scale TWBs

It is important to measure thickness variations across the stamped part especially in the areas of steep transitions. Some level of thinning is inevitable due to the nature of the process despite use of tailored drawing lubricants. To obtain thickness variations, non-destructive method of GOM scanning, non-contact optical metrology, technique was used to obtain full 3D profile of the parts. Figure 23 shows a colour heat map produced from the GOM scan data showing the thickness variations in selected heat-treated EBW TWBs after successful stamping operation. Figure 24 shows similar GOM scan data for selected heat-treated LBW TWBs. From these analysis, key outputs are summarised in Table 6. For similar material and sheet thickness TWBs, localised thinning is minimum for both EBW and LBW parts. The localised thinning is seen mainly in very small areas, especially corners, at the bottom most surface of stamped cruciform part.

The GOM scanning of the dissimilar heat-treated EBW and LBW TWBs showed varying degree of localised thinning, lowest (~16%) in similar weld of Al-6082 with 1.5 mm thickness and highest (~37%) in similar weld of Al-6082 with 2.5 mm thickness. Özdilli [35] carried out FE simulation of deep drawing of an engine oil pan part, a geometry that has some resemblance to the one used in the current work, with various sheet material data including steels and aluminium sheets. Of particular interest and relevance for the current work is results reported on Al-6082 (T6) material. It was reported that localised thinning in case of deep drawing of Al-6082 (T6) led to cracking for 1.5 mm sheet whereas for 2 mm sheet the maximum reported thinning was almost 65%. It is noteworthy that the Al-6082 (T6) used in Özdilli's work [35] did not receive any heat treatment prior to the deep drawing process. The process parameters used in the FE simulation, 3 mm/s velocity of a hydraulic press, are closely relevant to the ones used in the current work. This shows that the PWHT employed in the current work proves very effective in improving formability of Al-6082 (T6) and the level localised thinning observed after stamping is much improved. Authors are keen to carry out FE simulation work for the process and part geometry used in the current work with relevant material data to validate the results reported in this paper and report in a future publication.

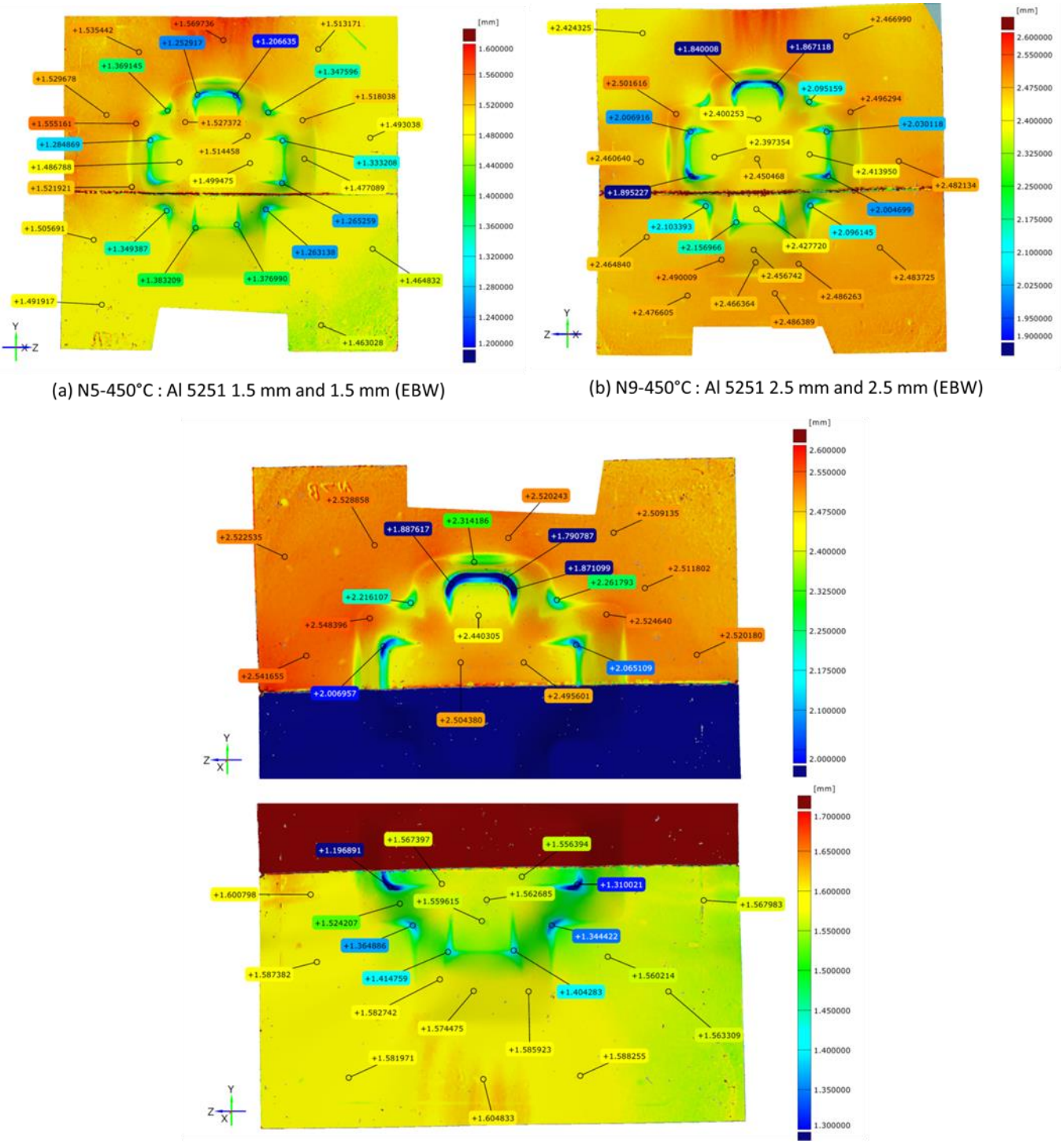

Figure 23: GOM scan results showing colour map of thickness variations in selected heat-treated EBW TWBs after stamping operation – (a) N5-450°C, (b) N9-450°C and (c) N7-450°C

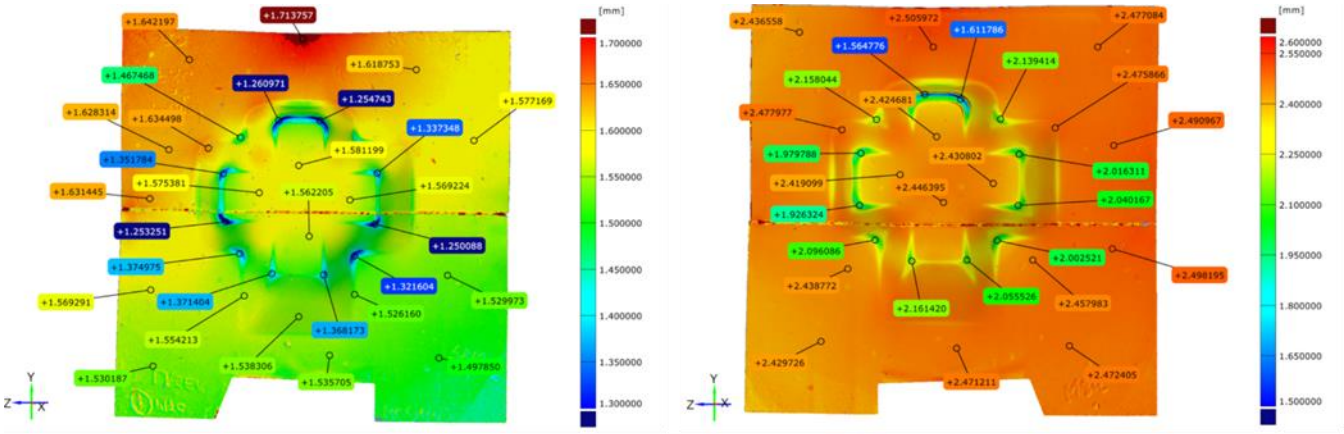

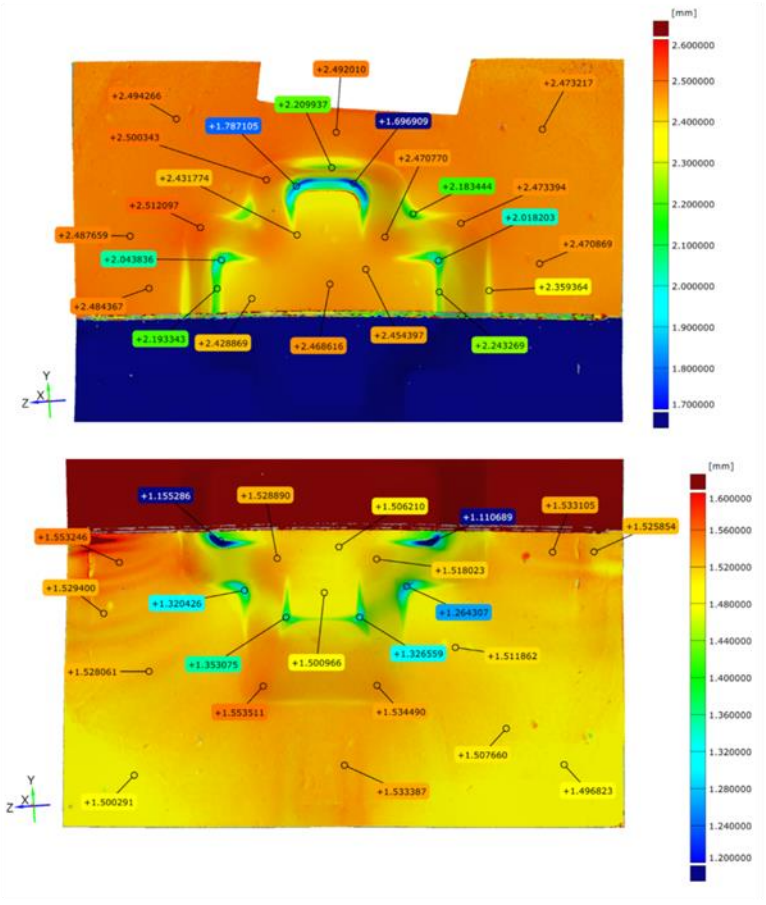

Figure 24: GOM scan results showing colour map of thickness variations in selected heat-treated LBW TWBs after stamping operation – (a) M1-450°C, (b) M8-450°C and (c) M3-450°C.

Table 6: Key outputs of the GOM scan data indicating thickness variations in selected heat-treated TWBs

Part ID	TWB description	Nominal thickness (mm)	Measured minimum thickness (mm)	Localised thinning (%)
N5 – 450ºC	Similar joint of Al-5251 (H22)	1.5 each	1.2	~20%
N9 – 450ºC	Similar joint of Al-5251 (H22)	2.5 each	1.84	~26%
N7 – 450ºC	Dissimilar joint of Al-5251(H22) and Al-6082(T6)	1.5 and 2.5	1.2 and 1.79	~20% and ~28%
M1 – 450ºC	Similar joint of Al-6082(T6)	1.5 each	1.25	~16%
M8 – 450ºC	Similar joint of Al-6082(T6)	2.5 each	1.56	~37%
M3 – 450ºC	Similar joint of Al-6082(T6)	1.5 and 2.5	1.11 and 1.69	~26% and ~32%

5. Conclusions

Following conclusions are drawn from this study:

- The LBW and the EBW processes are effective for manufacture of Al-5251 (H22) and Al-6082 (T6) TWBs with both similar and dissimilar material and thickness combinations. Attempts of stamping asR TWBs at the room temperature resulted in severe cracking at the weld and in the parent materials for all combinations of TWBs. This is attributed to residual stresses generated by the welding processes as well as the marked differences in the mechanical properties of two alloys used in the current work, especially in the H22 temper for the Al-5251 and the T6 temper for the Al-6082, which make these alloys much stronger but less formable.
- The PWHT at 450ºC for 30 minutes was sufficient in imparting stress relief to all the combinations of the TWBs produced from both processes allowing successful stamping of the TWBs. The heat treatment reduced peak load, also evident from reduced hardness, and increased elongation for the Al-5251 material by providing additional annealing. For the Al-6082 the PWHT caused additional aging resulting in softening. For both the materials the heat treatment also caused drop in hardness by static recovery relieving the residual stresses that are usually caused by the welding processes employed homogenizing the hardness distribution across the weld and in the parent materials as a result.
- The cold formed TWBs, after the PWHT, exhibited minimal thinning across the cruciform shaped final part except in much localised regions with the steepest angled walls where the maximum thinning reached to 37% for the case of similar material and thickness weld between Al-6082 sheets with 2.5mm thickness.

Acknowledgement

The authors are grateful to High value manufacturing Catapult (HVMC) for funding this work from their Innovate UK grant 160080 (core grant 2018 – 2023). The authors are thankful to Thomas Dutilleul of Nuclear Advanced Manufacturing Research Centre (NAMRC), Sheffield, UK and Bernd Baufeld of pro-beam technologies GMBH (previously at NAMRC) for providing EBW TWBs following sub-scale optimization trials. The authors are also thankful to Richard Jessett (previously at Manufacturing Technology Centre – MTC, Coventry, UK) for providing LBW TWBs following sub-scale optimization trials.

Author contribution

Himanshu Lalvani, as the principal investigator, secured funding for the project from the HVMC and led the work, coordinated experimental work with colleagues from NAMRC and MTC. Paranjayee Mandal, as the co-investigator, collated experimental data and analysed them to develop the manuscript.

References

[1] Hovanski Y, Upadhyay P, Pilli S, Carlson B, Carsley J, Hartfield-Wunsch S, et al. Aluminum Tailor-Welded Blanks for High Volume Automotive Applications. Light Met 2014 2014;9781118889:265–70. https://doi.org/10.1002/9781118888438.ch46.

[2] Parente M, Safdarian R, Santos AD, Loureiro A, Vilaca P, Jorge RMN. A study on the formability of aluminum tailor welded blanks produced by friction stir welding. Int J Adv Manuf Technol 2016;83:2129–41. https://doi.org/10.1007/s00170-015-7950-0.

[3] Pallett RJ, Lark RJ. The use of tailored blanks in the manufacture of construction components. J Mater Process Technol 2001;117:249–54. https://doi.org/10.1016/S0924-0136(01)01124-4.

[4] Lutsey N. Research Report – UCD-ITS-RR-10-10 Review of Technical Literature and Trends Related to Automobile Mass-Reduction Technology May 2010 2015.

[5] Mao, T., Altan T. Aluminum sheet forming for automotive applications, Part I Material properties and design guidelines. Stamp J 2013;1:12–3.

[6] Huntington CA, Eagar TW. Laser Welding of Aluminum and Aluminum Alloys. Weld J (Miami, Fla) 1983;62:1105–7.

[7] Pastor M, Zhao H, Martukanitz RP, Debroy T. Porosity, underfill and magnesium loss during continuous wave Nd:YAG laser welding of thin plates of aluminum alloys 5182 and 5754. Weld J (Miami, Fla) 1999;78.

[8] G Verhaeghe. LASER WELDING AUTOMOTIVE STEEL AND ALUMINIUM. 'Lasers Automot Sheet Met Ind TWI, Gt Abington, UK 2000.

[9] Venkat S, Albright CE, Ramasamy S, Hurley JP. CO2 laser beam welding of aluminum 5754-O and 6111-T4 alloys. Weld J (Miami, Fla) 1997;76:275-s.

[10] Braun R. Nd:YAG laser butt welding of AA6013 using silicon and magnesium containing filler

powders. Mater Sci Eng A 2006;426:250–62. https://doi.org/10.1016/j.msea.2006.04.033.

[11] Fabrègue D, Deschamps A, Suéry M. Influence of the silicon content on the mechanical properties of AA6xxx laser welds. Mater Sci Eng A 2009;506:157–64. https://doi.org/10.1016/j.msea.2008.11.033.

[12] Pakdil M, Çam G, Koçak M, Erim S. Microstructural and mechanical characterization of laser beam welded AA6056 Al-alloy. Mater Sci Eng A 2011;528:7350–6. https://doi.org/10.1016/j.msea.2011.06.010.

[13] Çam G, Ventzke V, Dos Santos JF, Koçak M, Jennequin G, Gonthier-Maurin P. Characterisation of electron beam welded aluminium alloys. Sci Technol Weld Join 1999;4:317–23. https://doi.org/10.1179/136217199101537941.

[14] Zhan X, Chen J, Liu J, Wei Y, Zhou J, Meng Y. Microstructure and magnesium burning loss behavior of AA6061 electron beam welding joints. Mater Des 2016;99:449–58. https://doi.org/10.1016/j.matdes.2016.03.058.

[15] Zhan X, Yu H, Feng X, Pan P, Liu Z. A comparative study on laser beam and electron beam welding of 5A06 aluminum alloy. Mater Res Express 2019;6. https://doi.org/10.1088/2053-1591/ab0562.

[16] Deschamps A, Ringeval S, Texier G, Delfaut-Durut L. Quantitative characterization of the microstructure of an electron-beam welded medium strength Al-Zn-Mg alloy. Mater Sci Eng A 2009;517:361–8. https://doi.org/10.1016/j.msea.2009.03.088.

[17] Mishra RS, Ma ZY. Friction stir welding and processing. Mater Sci Eng R Reports 2005;50:1–78. https://doi.org/10.1016/j.mser.2005.07.001.

[18] Threadgill, P L; Leonard, A J; Shercliff, H R; Withers PJ. FRICTION STIR WELDING OF ALUMINIUM ALLOYS. Int Mater Rev 2009;54:49–93.

[19] TWI. Job Knowledge 21. Alum Alloy 1996:1.

[20] Mossman MM, Lippold JC. Weldability testing of dissimilar combinations of 5000- and 6000-series aluminum alloys. Weld J (Miami, Fla) 2002;81.

[21] Soundararajan V, Yarrapareddy E, Kovacevic R. Investigation of the friction stir lap welding of aluminum alloys AA 5182 and AA 6022. J Mater Eng Perform 2007;16:484–91. https://doi.org/10.1007/s11665-007-9081-8.

[22] Costa MI, Verdera D, Leitão C, Rodrigues DM. Dissimilar friction stir lap welding of AA 5754-H22/AA 6082-T6 aluminium alloys: Influence of material properties and tool geometry on weld strength. Mater Des 2015;87:721–31. https://doi.org/10.1016/j.matdes.2015.08.066.

[23] Leitão C, Emílio B, Chaparro BM, Rodrigues DM. Formability of similar and dissimilar friction stir welded AA 5182-H111 and AA 6016-T4 tailored blanks. Mater Des 2009;30:3235–42. https://doi.org/10.1016/j.matdes.2008.12.005.

[24] Humberto Mota de Siqueira R, Capella de Oliveira A, Riva R, Jorge Abdalla A, Sérgio Fernandes de Lima M. Comparing mechanical behaviour of aluminium welds produced by laser beam welding (LBW), friction stir welding (FSW), and riveting for aeronautical structures. Weld Int 2016;30:497–503. https://doi.org/10.1080/09507116.2015.1096501.

[25] Lakshminarayanan AK, Balasubramanian V. Comparison of electron beam and friction stir weldments of modified 12wt% ferritic stainless steel. Mater Manuf Process 2011;26:868–77. https://doi.org/10.1080/10426914.2010.515643.

[26] TWI. WHAT IS THE DIFFERENCE BETWEEN HEAT INPUT AND ARC ENERGY? WHAT IS Differ BETWEEN HEAT INPUT ARC ENERGY? n.d. https://www.twi-global.com/technical-knowledge/faqs/faq-what-is-the-difference-between-heat-input-and-arc-

energy.

[27] Bardel D, Nelias D, Robin V, Pirling T, Boulnat X, Perez M. Residual stresses induced by electron beam welding in a 6061 aluminium alloy. J Mater Process Technol 2016;235:1–12. https://doi.org/10.1016/j.jmatprotec.2016.04.013.

[28] Zain-ul-abdein M, Nélias D, Jullien JF, Deloison D. Experimental investigation and finite element simulation of laser beam welding induced residual stresses and distortions in thin sheets of AA 6056-T4. Mater Sci Eng A 2010;527:3025–39. https://doi.org/10.1016/j.msea.2010.01.054.

[29] 1st Choice Metals. Aluminium 5000 Series Information Guide n.d.

[30] Smiths Metal Centres. 5251 (NS4) Technical Datasheet n.d.

[31] Aginagalde A, Gomez X, Galdos L, García C. Heat treatment selection and forming strategies for 6082 aluminum alloy. J Eng Mater Technol Trans ASME 2009;131:0445011–5. https://doi.org/10.1115/1.3120384.

[32] ASTM International. Standard Test Method for Knoop and Vickers Hardness of Materials (Designation: E384 − 11) 2015.

[33] Struers. Metallographic preparation of Aluminium and Aluminium alloys. Struers Appl Notes n.d. https://publications.struers.com/brochures/english/application-notes/aluminium/?_ga=2.201436953.982883093.1622030622-464541127.1622030622.

[34] F.J. Humphreys; M. Hatherly; Recrystallization and Related Annealing Phenomena. 1st Editio. Pergamon; n.d.

[35] ÖZDİLLİ Ö. An Investigation of the Effects of a Sheet Material Type and Thickness Selection on Formability in the Production of the Engine Oil Pan with the Deep Drawing Method. Int J Automot Sci Technol 2020;4:198–205. https://doi.org/10.30939/ijastech..773926.